2015

Supported metal complexes: From mesoporous silica to 3D printed polymers

Jacob Fleckenstein
Iowa State University

Supported metal complexes: From mesoporous silica to 3D printed polymers

by

Jacob Eran Fleckenstein

A thesis submitted to the graduate faculty

in partial fulfillment of the requirements for the degree of

MASTER OF SCIENCE

Major: Organic Chemistry

Program of Study Committee:
Aaron D. Sadow, Major Professor
Igor Slowing
Theresa Windus

Iowa State University

Ames, Iowa

2015

Dedicated to my wife Sara and to my family

TABLE OF CONTENTS

ACKNOWLEDGEMENTS

I would like to thank my advisor, Prof. Aaron Sadow. You were always pushing me to go further, keep trying, and keep moving forward even after reactions kept failing. Thank you to my committee members, Dr. Igor Slowing and Theresa Windus, for guiding me through my graduate career. Thank you especially to Dr. Igor Slowing who has collaborated with me on the majority of my projects.

Thank you to all of the Sadow group members, past and present. I have learned so much from you. A special thank you to Naresh Eedugurala who put up with all of my questions and helped me get started with my MSN projects. Thank you to Sebastian Manzano who provided me with the MSN I needed and also for the solid state characterization that was done on my catalyst complexes. Thank you to Sarah Cady and Shu Xu from instrument services for their help in the characterization of my products and compounds.

I'd like to thank my family and friends who have stood by me throughout my time in graduate school and supported me with the decisions I made. Thank you to my Grandfather who was a PhD chemist and who inspired me to go into chemistry. I wish he could have been here to see me graduate. A huge thank you to my wife, Sara, who always kept me positive and was the strength I needed to accomplish this achievement.

ABSTRACT

The drive to find heterogeneous catalysts for known and new reactions is of great interest. This interest comes from the increase in stability of the catalyst, the ease of separation from the reaction, and the ability to reuse the catalyst. In recent years, mesoporous silica has emerged as a very beneficial support for catalysts due to its highly Si-OH rich surface and immense surface area per gram.

A new zinc complex supported on the surface of SBA-15 type mesoporous silica nanoparticles (MSN) has been discovered. This system thus far been tested for hydrosilylation of carbonyl containing compounds and epoxidation of α, β-unsaturated ketones. The deprotonation of silanols on the surface of MSN with $ZnEt_2$ leads to the immobilization of ZnEt on the surface of MSN (MSN-ZnEt). Suspending MSN-ZnEt in an alcoholic solvent will lead to the corresponding MSN-ZnOR. MSN-ZnEt, MSN-ZnOEt, MSN-ZnO^{t}Bu and MSN-ZnOO^{t}Bu. Each of these MSN-Zn complexes have been isolated. MSN-ZnEt and MSN-ZnOEt have been characterized with FTIR, ICP-OES, BET, chemisorption, and TEM.

In the last few years additive manufacturing has begun to be incorporated into the chemical world by 3D printing custom chemical reactors for specific reactions and functionalized filament. We have successfully used stereolithography (SLA) three-dimensional (3D) printing, which photopolymerizes acrylic resin into a solid polymer, to create catalyst inserts that vary in surface area and contain a transition metal catalyst. Also, we have used SLA printing to create a unique reactor design to allow gas to flow into the vessel and hold up to 5 bar of pressure while also being able to release this pressure safely.

CHAPTER 1

INTRODUCTION

General Introduction

Heterogeneous Hydrosilylation

Catalytic reduction of various functional groups is a fundamental part of organic synthesis. Transition metal complexes have been used quite efficiently as catalysts for hydrogenations, hydrosilylations, and hydroborations, however, there are still limitations that require further advances. Some of the most active metals such as Pd, Rh, and Ir are also some of the most expensive and rare.[1] Currently the prices for Pd, Rh, and Ir are $698/oz, $955/oz, and $565/oz respectively[2] compared to zinc which is $0.06/oz.[3] This price differential is enough of a driving force to find new and effective ways to incorporate zinc into organometallic catalysis. In addition, zinc is abundant (making up 0.0078% of the earth's crust) and a non-toxic metal (having a daily dose for humans of 12-15 mg).[4]

In recent years, new catalytic uses for zinc has been heavily researched. Zinc complexes are effective catalysts for the asymmetric hydrosilylation of ketones,[5] reductive amination,[6] reduction of amides,[7] dehydrocoupling of silanes and alcohols,[8] reduction of CO_2,[9] epoxidation of enones,[10] and hydroamination.[11] However, all of these are examples of homogeneous catalysis. Discovering ways to use these important homogeneous examples to further heterogeneous research is crucial as 90% of the chemical industry is based on heterogeneous catalytic processes.[12] The basis of this percentage comes from the increased stability of the immobilized catalyst often leading to longer lasting catalysts, easy separation of the catalyst from the reaction, and the ability to recycle the catalyst. However, heterogeneous catalysts have some

significant limitations. These limitations include a low number of active sites, difficulty of understanding surface mechanisms, inadequacy of the techniques of surface characterization with respect to the real need for comprehension in a molecular way, difficulty of finding structure-activity relationships, and a purely empirical approach to the improvement of catalysts.[12] Majority of these limitations comes from the inability to use common characterization techniques, such as liquid phase NMR and single-crystal X-ray diffraction. This leads to other techniques being more heavily relied upon to determine what chemical interactions are occurring on the surface. These techniques include solid-state NMR, infrared spectroscopy, chemisorption, ICP-OES, XPS, XAS and powder XRD. Not knowing the surface interactions also inhibits the ability to do mechanistic studies on catalytic reactions.

The synthesis and production of mesoporous silica such as MCM-41/48[13] and SBA-15[14] have been known for many years. The materials have been widely research due to the extremely high surface areas ranging from 100 - 1000 m^2 g^{-1}, flexible pore sizes, morphology, and chemical stability.[15] These silica materials are made up of tetrahedral $[SiO_4]^{4-}$ and the surface is composed of siloxane bridges (≡Si-O-Si≡) and silanols groups (≡SiOH).[16] Mesoporous silica materials can be functionalized by (i) introducing organoalkoxysilane precursors during the co-condensation reactions (Scheme 1), (ii) grafting directly onto the mesopore surface (Scheme 2).[17]

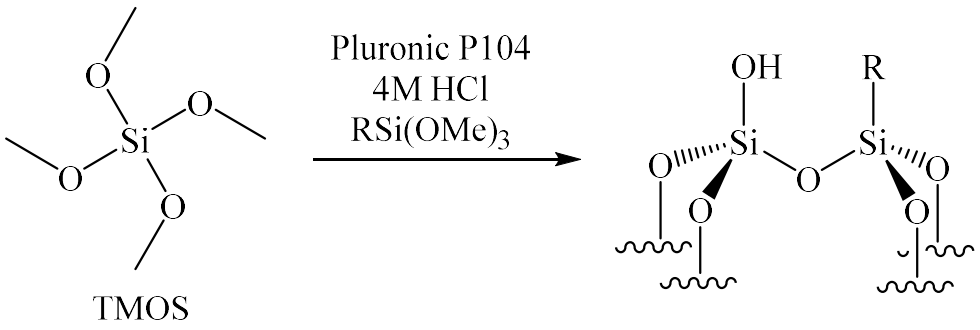

Scheme 1 Co-condensation of SBA-15 type mesoporous materials

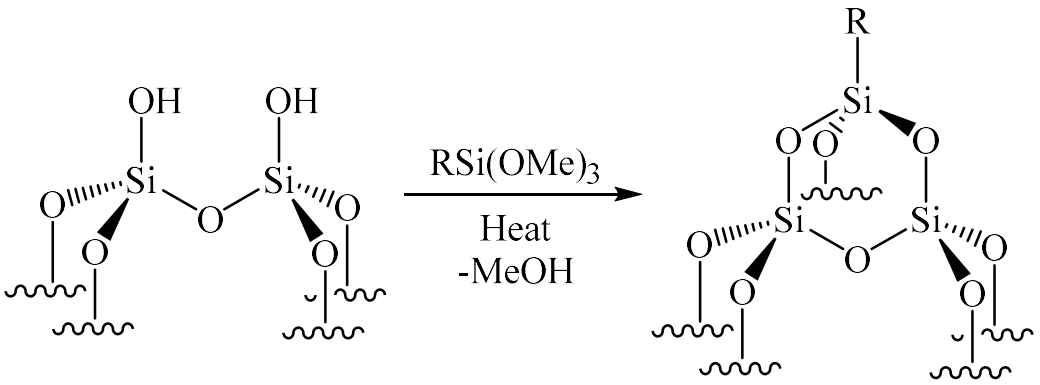

Scheme 2 Grafting of organoalkoxysilane on the mesopore surface

The grafting method seen in Scheme 2 is possible due to the silanols on the surface of the mesoporous silica. The organoalkoxysilane is able to react with the Si-OH bonds producing methanol and binding the R-Si to the surface. This is a very useful method as you are theoretically able to graft any organic complex on the surface and avoid the harsh conditions present during the co-condensation method. However, the limitation of grafting is that the organoalkoxysilane can build up on the surface and the openings of the pores and therefore not being homogeneously dispersed over the entire surface.[17] The alternative co-condensation method allows for homogeneity throughout the surface but as stated before requires harsh conditions.

Single-site heterogeneous catalysts bound to silica have been known for some time.[16-17] Some examples of these metal complexes bound to the surface of silica range from Re-, Mo- and W- imido olefin metathesis catalysts.[18-20] These catalysts are grafted onto the surface where a M-C bond is being replaced by a M-O bond and producing a hydrocarbon or amines in the Mo and W cases (Scheme 3).

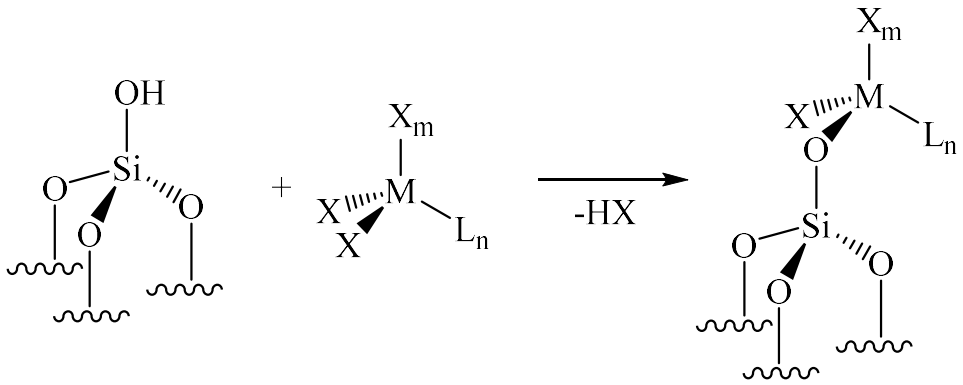

Scheme 3 Grafting of metals onto the surface of silica

This same interaction seen in Scheme 3 could then be applied to ZnR_2 and $Zn(OR)_2$ where HR and HOR would be produced respectively. This interaction involving ZnR_2 and $Zn(OR)_2$ has not been previously reported. The only known example of zinc directly bound to silica through and Si-O-Zn bond comes from Hock and co-workers showing the immobilization of zinc on the surface of silica for the hydrogenation of propylene and the dehydrogenation of propane.[21] $Zn(NO_3)_2•6H_2O$ was reacted with silica in aqueous conditions in the presence of ammonium hydroxide to successfully get single-site Zn(II) on the surface of silica (Scheme 4). In using this silica-zinc complex they were able to catalyze the hydrogenation of propene at temperatures near 200 °C and then the reverse propane dehydrogenation at temperatures around 550 °C. This is the first example seen of the immobilization of zinc on the surface of silica. No other catalytic reactions have come from this system yet.

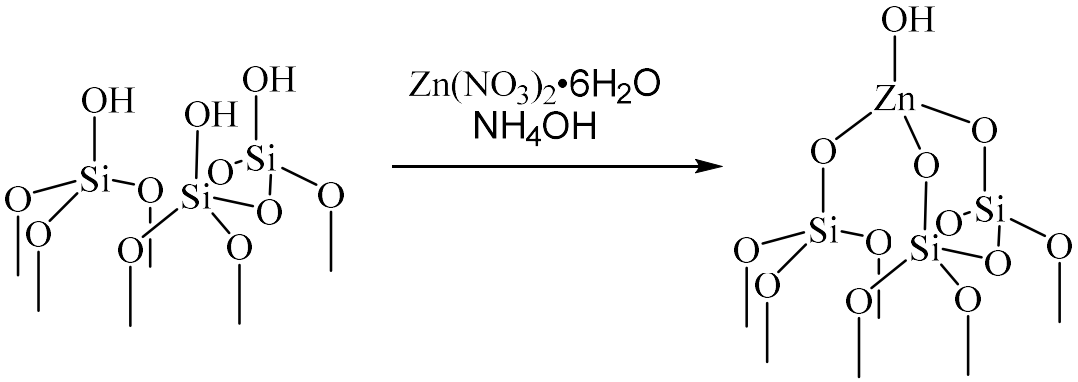

Scheme 4 Immobilization of zinc on the surface of silica

3D Printing

3D printing is a type of additive manufacturing that allows the user to create three dimensional objects that were designed in 3D drawing software. Currently there are multiple types of 3D printing but the most commonly used are fused deposition modeling (FDM), stereolithography (SLA), and selective laser sintering (SLS). FDM uses a plastic filament heated to its glass transition temperature and extruded in thin layers to create the 3D object. SLA uses a photo-reactive resin that polymerizes upon being treated with a UV laser. SLS uses a laser to sinter powdered metal. The powder is continuously sprayed while the laser sinters to create the 3D object. These technologies have been around for some time but only in recent years have they been used in the chemical world for printing functionalized filament and reactionware. Functionalizing the material being printed is a highly valuable ability. An example of which is use of the FDM method to print a conductive filament by mixing polycaprolactone and conductive carbon black filler for use as electronic sensors.[22]

The use of 3D printing in chemistry is in its infancy, although a few proof-of-principle examples have shown it is possible to print intricate reactors and dispense reactants and catalysts. Cronin and coworkers show the ability to 3D print a three section reaction vessel where each section is a different step of a reaction.[23] There remains many opportunities to harness the flexibility of 3D printing in the context of chemistry. An example of said opportunity is a catalyst integrated with the polymer that can be 3D printed into a shape or the reactor itself, which has not been done to the best of our knowledge. The incorporation of the catalyst into the print opens up many doors for use in chemical synthesis as a new way to incorporate catalysts into reactions.

References

1. Stephan Enthaler, Kathrin Junge, and Matthias Beller* *Angew. Chem. Int. Ed*. **2008**, *47*, 3317-3321.
2. www.platinum.matthey.com
3. www.vincentmetals.com
4. Stephan Enthaler* *ACS Catal*. **2013**, *3*, 150-158
5. a.) Hubert Mimoun,* Jeasn Yves de Saint Laumer, Luca Giannnini, Rosario Scopelliti, and Carlo Floriani *J. Am. Chem. Soc*. **1999**, *121*, 6158-6166. b.) Virginie Bette, André Mortreux,* Federico Ferioli, Gianluca Martelli, Diego Savoia,* and Jean-François Carpentier* *Eur. J. Org. Chem*. **2004**, 3040-3045. c.) Virginie Bette, André Mortreux, Diego Savoia, and Jean-François Carpentier* *Tetrahedron* **2004**, *60*, 2837-2842. d.) Virginie Bette, André Mortreux,* Diego Savoia, Jean-François Carpentier* *Adv. Synth. Catal*. **2005**, *347*, 289-302. e.) Jadwiga Gajewy, Marcin Kwit,* and Jacek Gawroński* *Adv. Synth. Catal*. **2009**, *351*, 1055-1063. f.) Stephan Enthaler,* Björn Eckhardt, Shigeyoshi Inoue, Elisabeth Irran, and Matthias Driess *Chem. Asian J*. **2010,** *5*, 2027-2035. g.) Shuai Liu, Jiajian Peng,* Hu Yang, Ying Bai, Jiayun Li, Guoqiao Lai* *Tetrahedron* **2012**, *68*, 1371-1375. h.) Wesley Sattler and Gerard Parkin* *J. Am. Chem. Soc*. **2012**, *134*, 17462-17465..
6. Stephan Enthaler *Catal. Lett*. **2011**, *141*, 55-61
7. Shoubhik Das, Daniele Addis, Kathrin Junge, and Matthias Beller* *Chem. Eur. J.* **2011**, *17*, 12186-12192.
8. Debabrata Mukherjee, Richard R. Thompson, Arkady Ellern, and Aaron D. Sadow* *ACS Catal*. **2011**, *1*, 698-702
9. Wesley Sattler and Gerard Parkin* *J. Am. Chem. Soc.* **2012**, *134*, 17462-17465

10. Michael J. Porter and John Skidmore *Chem Commun*. **2000**, 1215-1225

11. Anja Lühl, Larissa Hartenstein, Siegfried Blechert* and Peter W. Roesky* *Organometallics* **2012**, *31*, 7109-7116

12. Christophe Copéret,* Mathieu Chabanas, Romain Petroff Saint-Arroman, and Jean-Marie Basset* *Angew. Chem. Int. Ed*. **2003**, *42*, 156-181.

13. a.) J.S. Beck,* J. C. Vartuli,* W. J. Roth,* M. E. Leonowicz,* C.T. Kresge,* K. D. Schmett, C. T-W. Chu, D. H. Olsen, E. W. Sheppard, S. B. McCullen, J. B. Higgins, and J. L. Schlenker *J. Am. Chem. Soc.* **1992**, *114*, 10834-10843. b.) C. T. Kresge, M. E. Leonowicz, W. J. Roth, J. C. Vartuli, J. S. Beck *J. S. Nature (London).* **1992**, *359*, 710-712

14. D. Zhao, J. Feng, Q. Huo, N. Melosh, G. H. Frederickson, B. F. Chmelka, G. D. Stucky, *Science (Washington, D. C.)* **1998**, *279*, 548-552

15. a.) Igor I. Slowing, Brian G. Trewyn, Supratim Giri, and Victor S.-Y. Lin* Adv. Funct. Mater. 2007, 17, 1225-1236. b.) Seong Huh, Jerzy W. Wiench, Brian G. Trewyn, Seahn Song, Marek Pruski, and Victor S.-Y. Lin* *Chem. Comm*. **2003**, 2364-2365. c.) Isa K. Mbaraka, Daniela R. Radu, Victor S.-Y Lin, and Brent H. Shanks* *J. Catalysis* **2003**, *219*, 329-336

16. Fernando Rascón, Raphael Wischert and Christophe Copéret* *Chem. Sci.* **2011**, *2*, 1449-1456

17. Seong Huh, Jerzy W. Wiench, Ji-Chul Yoo, Marek Pruski, and Victor S.-Y. Lin* *Chem. Mater.* **2003**, *15*, 4247-4256

18. Mathieu Chabanas, Anne Baudouin, Christophe Copéret,* and Jean-Marie Basset* *J. Am. Chem. Soc.* **2001**, *123*, 2062-2063

19. Frédéric Blanc, Christophe Copéret, Jean Thivolle-Cazat, Jean-Marie Basset, Anne Lesage, Lyndon Emsley, Amritanshu Sinha and Richard R. Schrock* *Angew. Chem. Int. Ed*. **2006**, *8*, 1216-1220

20. Bouchra Rhers, Alain Salameh, Anne Baudouin, Elsje Alezzandra Quadrelli, Mostafa Taoufik, Christophe Copéret, Frédéric Lefebvre, Jean-Marie Basset, Xavier Solans-Monfort, Odile Eisenstein,* Wayne W. Lukens, Lordes Pia H. Lopez, Amritanshu Sinha, and Richard R. Schrok* *Organometallics*, **2006**, *25*, 3554-3557

21. Neil M. Schweitzer, Bo Hu, Ujjal Das, Hacksung Kim, Jeffery Greeley, Larry A. Curtiss, Perter C. Stair, Jeffrey T. Miller,* and Adam S. Hock* *ACS Catal*. **2014**, *4*, 1091-1098

22. Simon J. Leigh*, Robert J. Bradley, Christopher P. Purssell, Duncan R. Billson, and David A. Hutchins. *PLOS ONE*, **2012**, *7*, 1-6.

23. Philip J. Kitson, Mark D. Symes, Vincenza Dragone and Leroy Cronin*. *Chem. Sci*. **2013**, *4*, 3099-3103

CHAPTER 2

SYNTHESIS OF MSN-ZINC ALKYL AND ALKOXY COMPOUNDS, THEIR CHARACTERIZATION AND CATALYTIC ACTIVITY

Jacob Fleckenstein, Sebastián Manzano, Igor I. Slowing*, and Aaron D. Sadow*

Abstract

SBA-15 type mesoporous silica nanoparticles (MSN) have been successfully used as the solid support for a zinc alkoxide pre-catalyst for the hydrosilylation of carbonyl containing compounds with triethoxysilane and phenyl silane as the reducing agents. The immobilization of zinc on the surface of MSN was accomplished by the reaction of $ZnEt_2$ and partially dehydroxylated mesoporous silica resulting in MSN-ZnEt and ethane. This MSN zinc complex was further reacted with alcoholic solvents, such as ethanol and *tert*-butanol, in order to produce the corresponding MSN-ZnOR complexes. Control experiments of MSN, silane, and acetone were performed in order to show that in the absence of zinc no catalytic activity was witnessed. MSN-ZnOEt has been characterized using FTIR, ICP-OES, TEM and Powder XRD. This is the first example of a surface-supported ZnEt and also a heterogeneous zinc catalyst for the hydrosilylation of carbonyls.

The catalytic epoxidation of α,β-unsaturated ketones in the presence of *tert*-butyl hydroperoxide was also catalyzed by MSN-ZnOEt. Control experiments of MSN, tert-butyl hydroperoixde, and chalcone were performed and showed no catalytic epoxidation of chalcone. This catalyst has not been previously reported, and shows reactivity towards the epoxidation of *trans*-chalcone. In addition, zinc *tert*-butylperoxide was immobilized on MSN (MSN-ZnOO^{t}Bu) and isolated by reacting stoichiometric ammounts of MSN-ZnOEt with *tert*-butyl hydroperoxide.

§ Other authors' contributions

Sebastián Manzano: Synthesis of mesoporous silica and surface characterization of all MSN-Zn complexes

Igor I. Slowing: Help and advice with reactions involving mesoporous silica

Introduction

The catalytic reduction of carbonyls to form secondary alcohols is of great interest in organic synthesis.[1] A stoichiometric reduction using highly active metal hydrides such as $LiAlH_4$ and $NaBH_4$ has been a long standing method,[2-3] though major disadvantages accompany this method (i) functional group selectivity is low (ii) stoichiometric amounts of metal waste produced (iii) the mixture needs to be quenched after the reaction is complete. As an alternative, the catalytic reduction using silanes as the reducing agent in the presence of transition metals is a promising alternative. The homogeneous enantioselective hydrosilylation of ketones using various metals as catalysts such as Rh,[4] Ru,[5] Ir,[6] Ti,[7] Cu,[8] and Zn[9] has been extensively explored. Rh and Ir examples all result in high yields and high ee% for aliphatic and aromatic ketones while using Ph_2SiH_2 as the reducing agent. Ti and Cu also show high yields and high ee% for aromatic ketones only while using either Ph_2SiH_2 or PMHS as the reducing agent. However, the Ru examples show either high yields and low ee% or the opposite for aromatic ketones only. The Zn examples are promising, showing high yields and high ee% for aliphatic and aromatic ketones and also being able to use a range of silanes such as PMHS, $(EtO)_3SiH$, and $PhSiH_3$. It is believed that the reaction of zinc alkoxy complexes react with a silane to produce a zinc hydride which goes on to insert into a carbonyl bond and forming a zinc alkoxy species again. They hydride then gets reformed by reaction with another silane (Scheme 1).[9b,e,h]

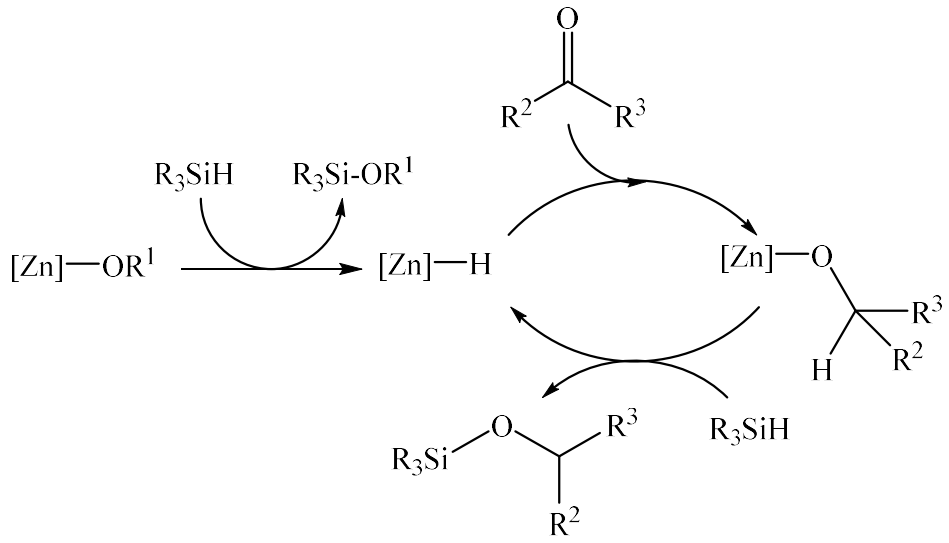

Scheme 1 Possible mechanism for the hydrosilylation of ketones

Examples of heterogeneous catalysis has been lacking, with only a few examples of a Rh-NHC catalyst immobilized on MCM-41being reported in the literature.[10] For this immobilization the NHC in question is functionalized with an isopropoxysilane group in order to be grafted onto the surface of silica (Scheme 2). This example shows high conversion of 99% of acetophenone to the corresponding alcohol. Though this system is promising with a high conversion rate there still are significant limitations such as a limited substrate scope of just acetophenone, air and moisture sensitive, and using an expensive and rare metal.

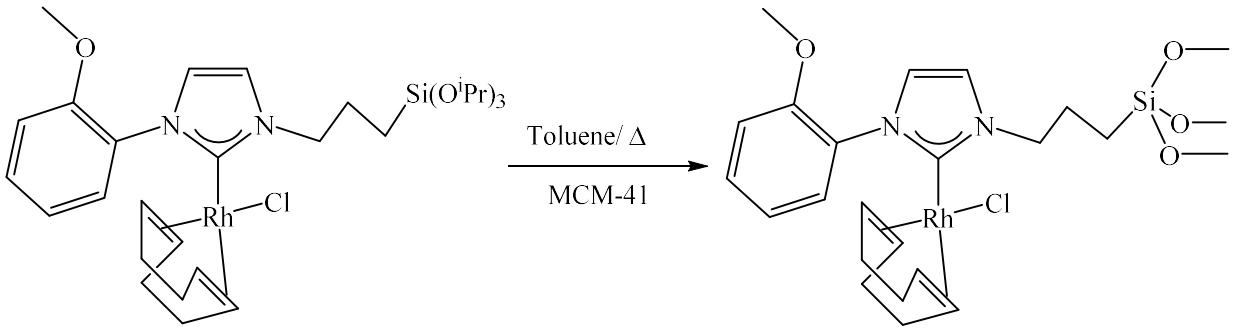

Scheme 2 Grafting of Rh-NHC on surface of MCM-41

Epoxides are of great importance when it comes to organic synthesis because they give rise to various 1,2-difunctionalized compounds.[11] As such Barry Sharpless was awarded the Nobel Prize in 2001 for his work in the field of asymmetric epoxidation (Scheme 3).[12]

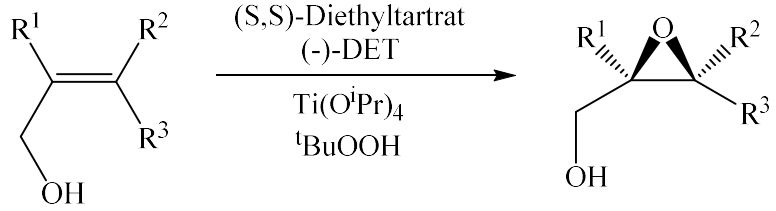

Scheme 3 Sharpless epoxidation using $Ti(O^iPr)_4$

Many transition metal complexes can be used in the catalytic epoxidation of olefins such as Mo, W, Re, and Mn.[13] However, Enders and coworkers have shown that zinc shows great reactivity towards the epoxidation of electron-deficient olefins giving yields of >94% and ee% of up to 92% (Scheme 4).[14]

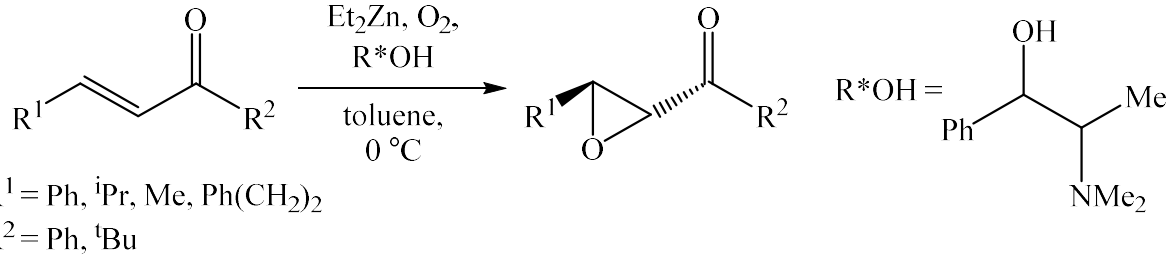

R^1 = Ph, ^{i}Pr, Me, $Ph(CH_2)_2$
R^2 = Ph, ^{t}Bu

Scheme 4 Catalytic epoxidation of electron deficient olefins using zinc

Another example of zinc epoxidation comes from Ding and coworkers. They use diethyl zinc and a binol ligand for the heterogeneous enantioselective epoxidation of chalcone with cumene hydroperoxide resulting in isolated yields up to 99% and ee% of up to 88% (Scheme 5).[15]

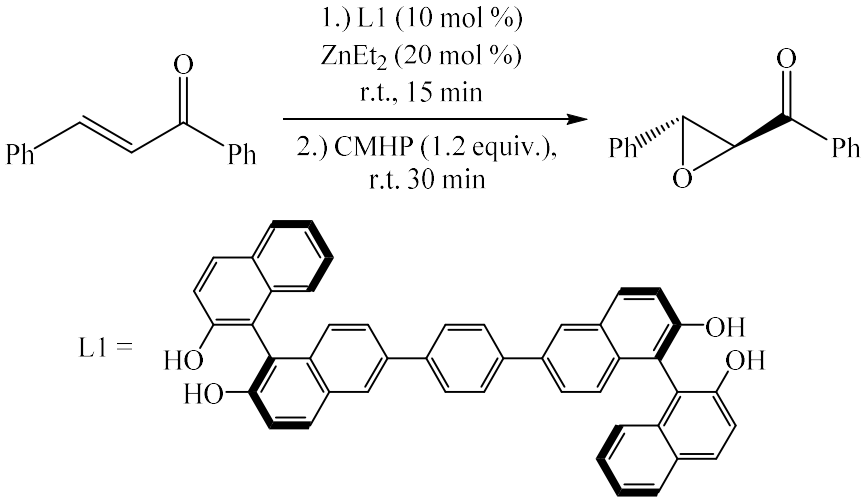

Scheme 5 Catalytic epoxidation of chalcone using a binol-Zn catalyst

Herein, we report the synthesis of the immobilization of ZnOEt onto the surface of MSN. To the best of our knowledge this is first example of a zinc catalyst for the heterogeneous hydrosilylation of ketones, aldehydes and esters. Several silanes were tested in this catalytic system as were different solvents and MSN-Zn complexes. The surface of MSN-ZnOEt was characterized using BET, ICP-OES, Powder XRD, and TEM. Also reported is the catalytic epoxidation of α,β-unsaturated ketones with *tert*-butylhydroperoxide using the same catalytic system.

Results and Discussion

$ZnEt_2$ and ZnH_2 are not active catalysts for the reduction of methyl benzoate by PMHS.[9a] The addition of diamine ligands such as ethylenediamine and tetramethylethylenediamine were required for zinc to be a successful catalyst. Enthaler and co-workers then showed 2,4,6-tri-tert-butylphenol was also successful in stabilizing zinc and was able to successfully reduce acetophenone with triethoxysilane as the reducing agent to get a 99% GC yield (Scheme 1).[9g]

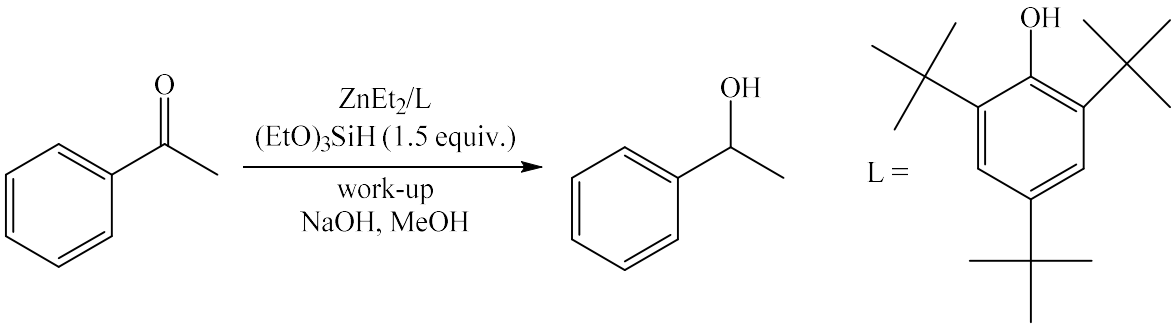

Scheme 1 Hydrosilylation of acetophenone using $ZnEt_2$ with a phenol ligand

We were curious, then, to see if Si-OH bonds on the surface of MSN could be used as a ligand for zinc and if MSN-ZnR or MSN-ZnOR could be a single-site catalyst for the hydrosilylation of ketones. Since, this immobilization has never been done before certain aspects needed to be tested. It was not known if the silanols on the surface would react with $ZnEt_2$ in a way that would produce ethane and bind ZnEt on the surface. It was uncertain that if the silanols were too dense on the surface a Si-O-Zn-O-Si bridge would form and if so would that zinc be catalytically active. Also, if an MSN-ZnR or MSN-ZnOR forms will the Si-O-Zn break upon addition of silane.

In order to start answering some of these questions the MSN to be used needed to be pretreated and characterized. The first step was to lower the amount of silanols on the surface of MSN by heating the MSN to 550 °C under reduced pressure for 12 h. Under the high heat, the silanols on the surface will condense to form siloxane bridges. The formation of these bridges releases water and in turn reduces the amount and overall density of silanols on the surface of MSN (Scheme 2).[16]

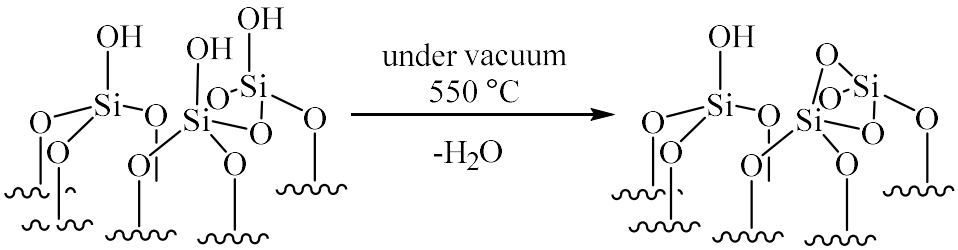

Scheme 2 Formation of siloxane bridges on the surface of MSN

To determine the amount of silanols present on the surface, MSN was reacted with dibenzyl magnesium to produce toluene (Scheme 3).[17] The amount of free Si-OH bonds could be then determined by quantifying the amount of toluene produced, since the ratio of toluene produced to silanols on the surface is 1:1. The result from this experiment indicated that the MSN being used for these reactions had a Si-OH loading of 1.93 mmol of Si-OH per gram of MSN.

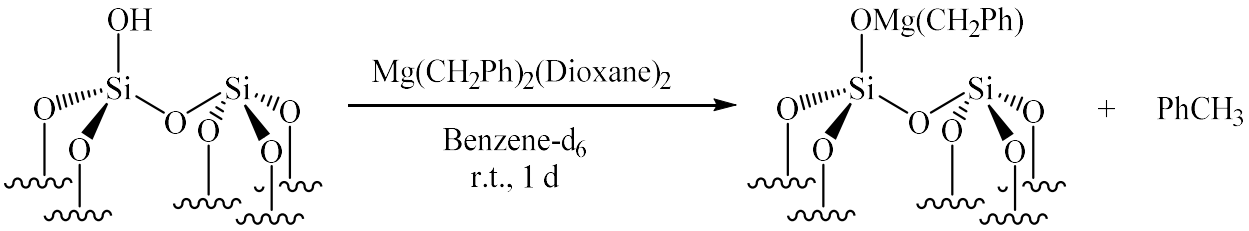

Scheme 3 Reaction of MSN with dibenzyl magnesium in order to determine Si-OH loading

MSN was then reacted with $ZnEt_2$ in order to form the MSN-ZnEt complex(Scheme 4). Bubbles were seen upon addition of $ZnEt_2$ and analysis by ^1H NMR determined that these bubbles were ethane being produced. Scheme 4 shows a monopodal MSN-ZnEt complex, however as stated before it is possible for the ZnEt bound to the surface to deprotonate another silanol producing a Si-O-Zn-O-Si bridge that is not shown.

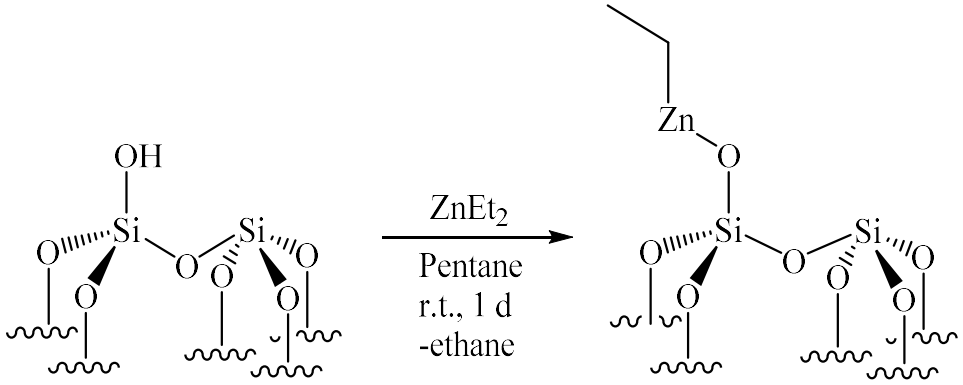

Scheme 4 Addtion of $ZnEt_2$ to get the MSN-ZnEt complex.

Upon formation of the MSN-ZnEt complex, it was thought that it would react with alcoholic solvents, such as EtOH and *tert*-butanol, in order to produce a MSN-ZnOR complex and ethane. The MSN-ZnEt was suspended in the solvent and let stir at room temperature for 1 d (Scheme 5). During this reaction bubbles were witnessed, so the reaction was done an NMR scale and the production of ethane was seen.

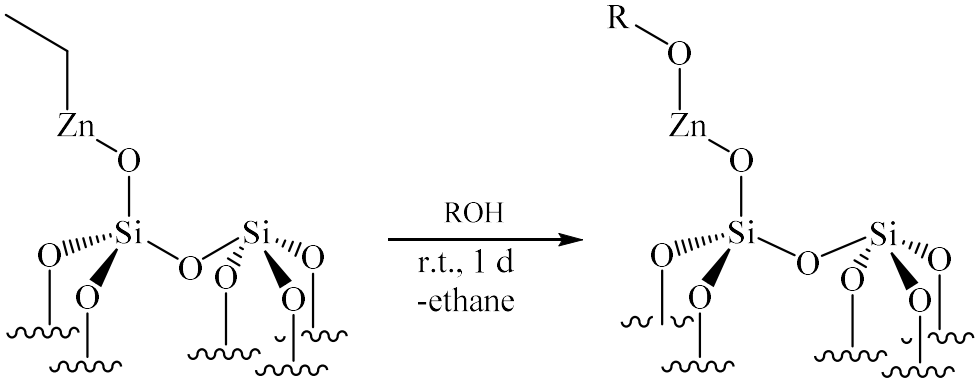

Scheme 5 Addition of alcohols to MSN-ZnEt in order to get MSN-ZnOR.

Once zinc was thought to be immobilized on the surface it was necessary to determine the zinc loading. ICP-OES was then used to determine the amount of mmol of zinc g^{-1} for MSN-ZnEt, MSN-ZnOEt, and MSN-ZnO^{t}Bu. With the addition of $ZnEt_2$ and the following reactions with EtOH and ^{t}BuOH it was found that MSN-ZnEt, MSN-ZnOEt, and MSN-ZnO^{t}Bu had zinc loadings of 0.866, 0.847, and 0.730 mmol/g respectively (Table 1). It is a concern that the zinc

loading in MSN-ZnO^{t}Bu showed a loss compared to the MSN-ZnEt loading. A possible explanation for this loss could be that the *tert*-butanol broke some of the Si-O-Zn bonds producing $Zn(O^tBu)_2$. The result from the ICP-OES showed that the zinc loading on MSN was significantly lower than the Si-OH loading of 1.93 mmol g^{-1}. Two possible reasons for this loss in loading could be that not all of the silanols reacted with $ZnEt_2$ or it could indicate that some of the zinc grafted on the surface is dipodal despite the efforts to reduce the density of silanols on the surface.

The MSN-Zn complexes were analyzed by BET in order to determine the surface area, pore volume, and pore size (Table 1). It was seen that after the grafting of ZnEt on the surface of MSN the surface area of the sample lowered almost 70 m^2/g, which was calculated by the amount of nitrogen that was adsorbed onto the surface. This results indicates that something was now occupying space on the surface and not allowing the nitrogen to be adsorbed. This idea was further enforced by the pore volume of the samples also decreasing from 0.936 to 0.786 mL/g.

Table 1. Surface characterization results from BET, ICP-OES and reaction with dibenzyl magnesium

Sample	Surface Area (m^2/g)	Pore Vol. (mL/g)	Pore Size (nm)	Zn Loading (mmol/g)	Si-OH Loading (mmol/g)
MSN	398.2	0.936	7.39	-	1.93
MSN-ZnEt	333.4	0.786	7.25	0.866	-
MSN-ZnOEt	328.0	0.790	7.40	0.847	-
MSN-ZnO^{t}Bu	343.3	0.776	7.21	0.730	-

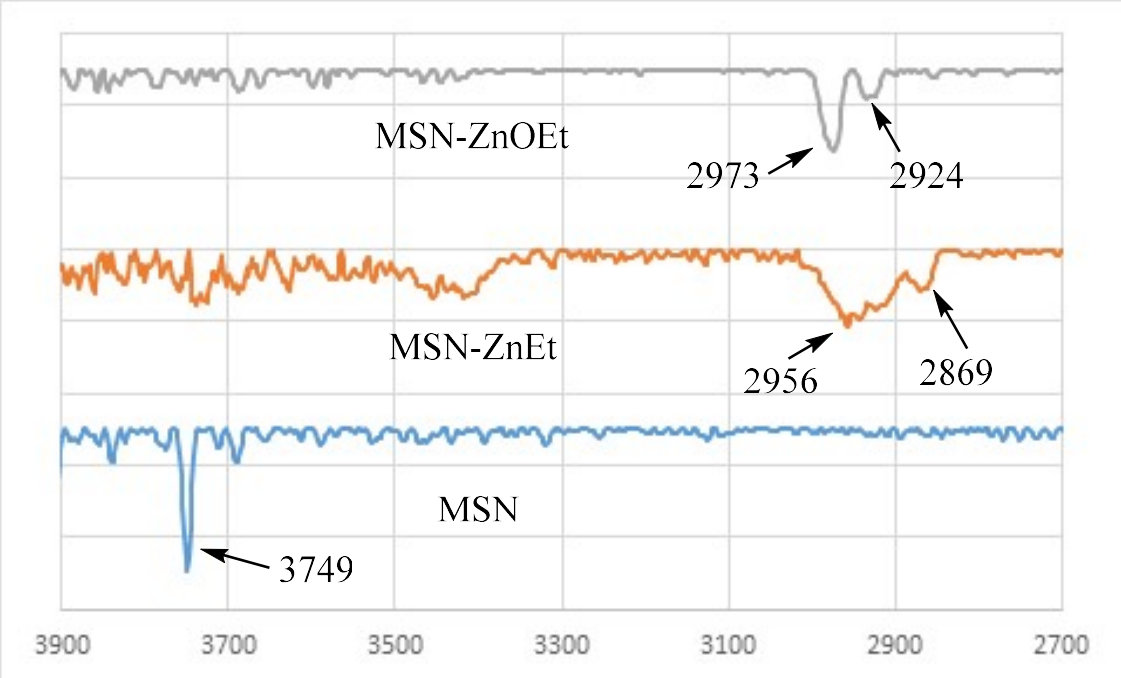

Figure 1. FTIR of MSN, MSN-ZnEt and MSN-ZnOEt using a KBr pellet.

To further characterize these complexes FTIR-spectroscopy was used to look for the C-H stretching of the ethyl groups on the surface (Figure 1). For MSN the important peak was the sharp one at 3789 cm^{-1}, indicating there are isolated Si-OH bonds on the surface and that no water is adsorbed on the surface. Small peaks then grow in once ZnEt and ZnOEt are immobilized on the surface as seen in Figure 1. It is noted that the C-H peaks shift between the ZnEt and ZnOEt complexes indicating that a change occurred on the surface.

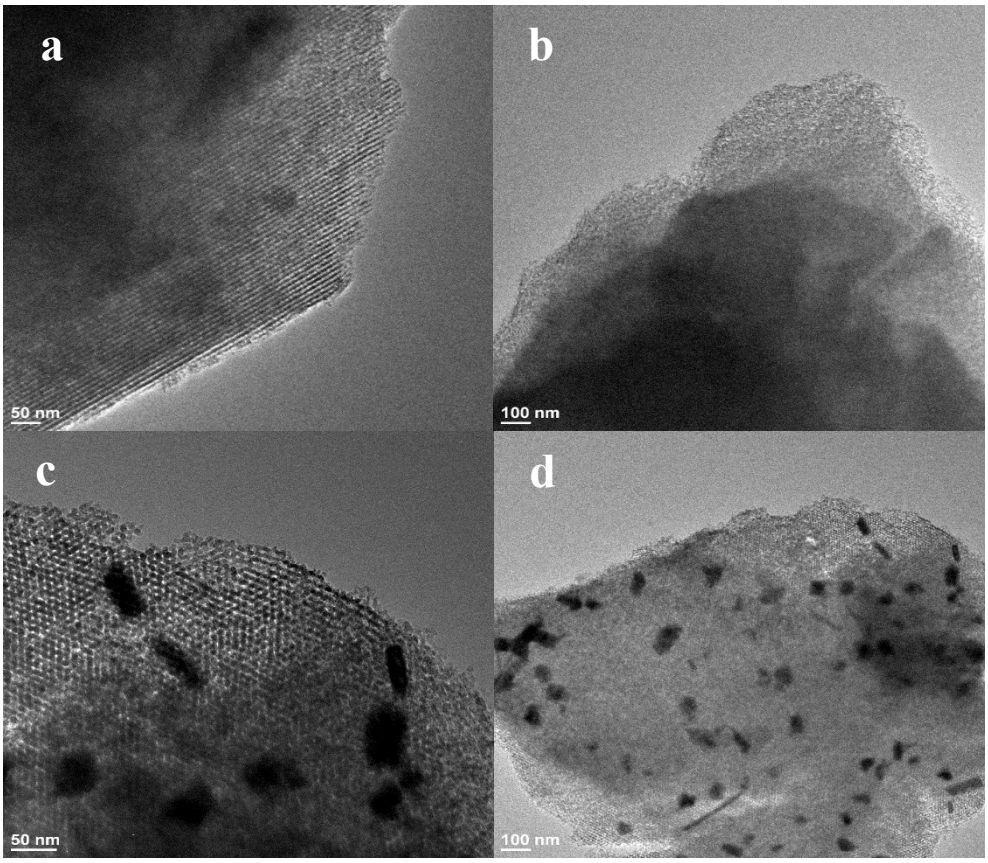

Figure 2. TEM images of MSN-Zn complexes. [a] MSN-ZnOEt 50 nm. [b] MSN-ZnOEt 100 nm. [c] MSN-ZnOEt + $PhSiH_3$ 50 nm. [d] MSN-ZnOEt + $PhSiH_3$ 50 nm.

TEM images were taken of the solid MSN-ZnOEt to determine if the zinc is homogeneously dispersed throughout the MSN. In Figures 2-a and 2-b it can be seen that there are no clumps of black indicating that the zinc on the MSN is not condensing on the surface but is evenly dispersed throughout the pores, which is the ideal result. The fact that the zinc is present on the solid and homogeneously spread out on the surface also gives the indication that the zinc is bound to the silanols. Images c and d in Figure 2 are the result of the background reaction of MSN-ZnOEt and $PhSiH_3$. Upon heating of MSN-ZnOEt and $PhSiH_3$ a color change occurs and the MSN would go from white to black in color suggesting some kind of decomposition of the zinc metal in the sample.

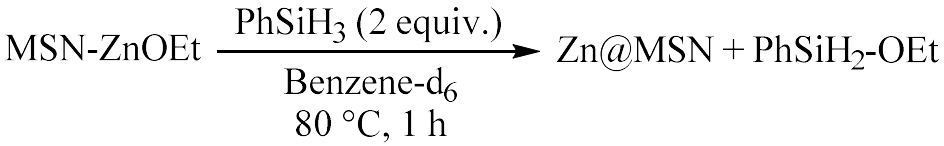

Scheme 6 Background reaction of MSN-ZnOEt with $PhSiH_3$ to form zinc nanoparticles on the surface of MSN

The TEM images, Figure 2 c and d, indicated that the ZnOEt on the surface is transformed into zinc nanoparticles on the surface of MSN. It is known that the reaction of $[To^M]ZnO^tBu$ and phenyl silane react to form $[To^M]ZnH$.[18] It is possible then that the reaction of MSN-ZnOEt and $PhSiH_3$ produces MSN-ZnH and $PhSiH_2$-OEt (Scheme 6). The excess $PhSiH_3$ in solution could then react with MSN-ZnH, breaking the Si-O-Zn bond and forming ZnH_2. The ZnH_2 would then decompose to zinc metal and hydrogen.

Powder X-Ray diffraction (XRD) results show that the rods are zinc nanoparticles and not ZnO nanoparticles (Figure 3). Figure 3 shows the peaks corresponding to those of zinc metal. When zinc oxide was compared only one of the peaks suggested zinc oxide was present. This decomposition of the MSN-ZnOEt is the main reason the hydrosilylation reactions use a stoichiometric amount of silane compared to other literature examples which use excess silane to speed up the reaction. It was difficult to use excess silane and stop the reaction before any Zn@MSN was formed. This was a problem because Zn@MSN is inactive for the hydrosilylation reactions.

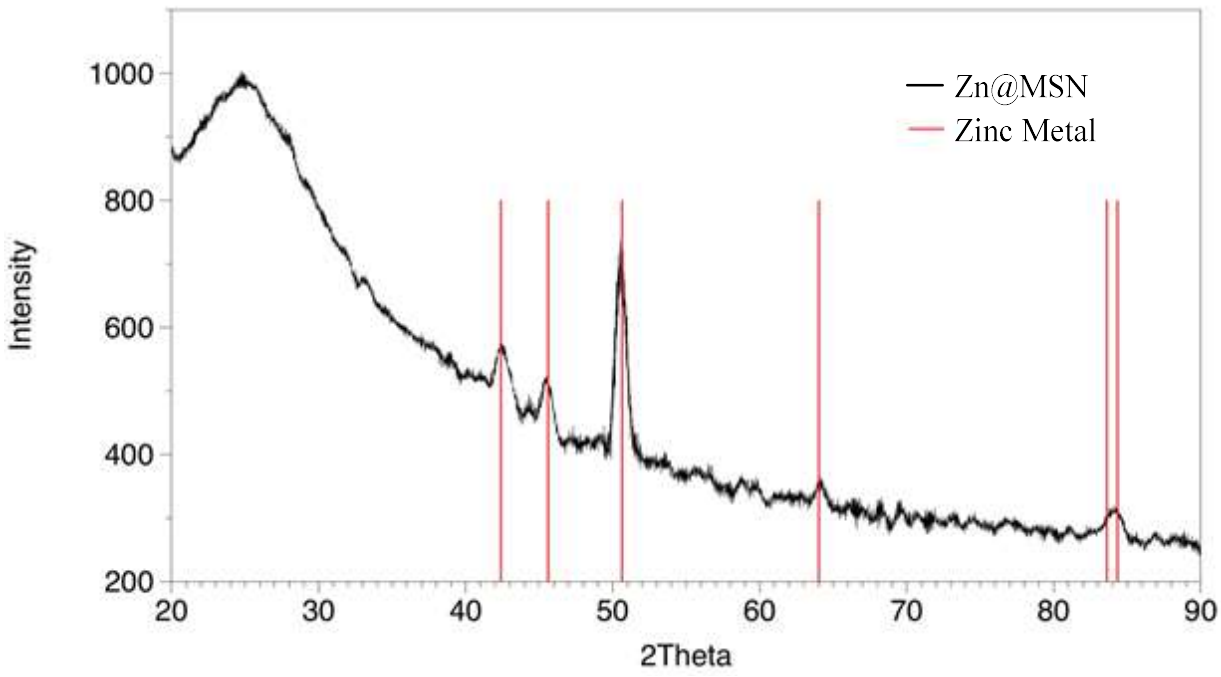

Figure 3 Powder XRD results of MSN-Zn nanoparticles.

We then wanted to start testing of different pre-catalyst complexes for the hydrosilylation of acetone using $PhSiH_3$ as the reducing agent (Table 2). We found MSN-ZnOEt gives full conversion of acetone and a decent yield of 65% determined by ^1H NMR. Given the same amount of time MSN-ZnEt and MSN-ZnO^{t}Bu only produced 93% and 87% conversion and 55% and 44% yield. However, in 4 hours both MSN-ZnEt and MSN-ZnO^{t}Bu showed full conversion. MSN-ZnOEt showed a higher activity compared to MSN-ZnEt and MSN-ZnO^{t}Bu in both percent conversion and yield so it was used as the pre-catalyst for the subsequent experiments. It is unknown at this time what the side products are explaining the loss in yield compared to conversion. The background reaction using un-functionalized MSN as the catalyst and $PhSiH_3$ as the reducing agent showed only acetone and $PhSiH_3$ after 16 hours at 60 ºC as was expected.

Table 2. Testing of zinc alkyls and zinc alkoxides bound to the surface of MSN. [a] Yield calculated by ^{1}H NMR spectroscopy using an internal standard.

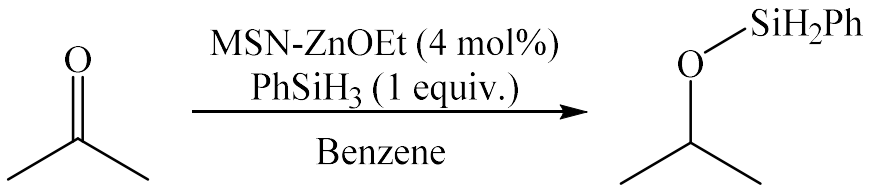

Pre-Catalyst	Time	Temp (°C)	Conv. (%)	Yield[a] (%)
MSN-ZnEt	3 h	60	93	55
MSN-ZnOEt	3 h	60	100	65
MSN-ZnO^{t}Bu	3 h	60	87	44
MSN	16 h	60	-	-

From literature examples involving hydrosilylation in the presence of zinc, toluene was the most often used solvent. We then did a couple quick experiments to see if toluene was indeed the best solvent for our system (Table 3). However, during these experiments it was determined that no solvent effect was seen between the solvents chosen. Benzene, toluene, and methylene chloride all gave 100% conversion of acetone within similar amounts of time and the yields were very close at 65, 69, and 67% respectively. Methylene chloride was slightly faster but due to price differential and availability in our lab we decided to use benzene as the solvent for NMR scale reactions from here on out.

As stated in the introduction, the only known example of a heterogeneous hydrosilylation catalyst comes from Lázaro et al. and is highly air and moisture sensitive.[10] Also, majority of homogeneous hydrosilylation examples involving zinc are also air and moisture sensitive because their catalysts are formed in situ using $ZnEt_2$.[9b-g] We then wanted to determine if our system had the same limitations. The same hydrosilylation of acetone with $PhSiH_3$ as the reducing agent was attempted except this time it was done under air and with wet benzene-d_6.

The reaction took a longer amount of time at 4 h and gave a slightly less percent yield of 58% but it is clear that MSN-ZnOEt is catalytically active in the presence of air and water.

Table 3. Testing for solvent effect on the hydrosilylation of acetone. [a] Yields were calculated using ^{1}H-NMR.

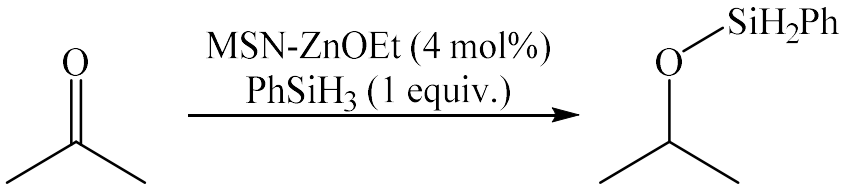

Solvent	Time	Temp (°C)	Conv. (%)	Yield[a] (%)
C_6D_6	3 h	60	100	65
Tol-d_8	3 h	60	100	69
CD_2Cl_2	2 h	60	100	67
C_6D_6 - wet	4 h	60	100	58

Another variant of hydrosilylation of ketones in the literature are the different silanes that are used for different systems.[4-9] Majority of Rh, Ir, Ru, Ti, and Cu systems use secondary silanes such as $PhSiH_2$. However, the examples involving Zn use tertiary silanes such as polymethylhydrosiloxane (PMHS) and triethoxysilane, though primary and secondary silanes were still reactive.[9] Several silanes were tested in the reduction of acetone to the corresponding silylether in order to determine the silane that would give the fastest rates and highest conversion and yields (Table 4). The first property tested was to see if primary, secondary, or tertiary silanes had an effect on the reaction. $PhSiH_3$ gives full conversion of acetone in 3 h at 60 ºC where as $PhMeSiH_2$ and Et_3SiH gave much less promising results (Entries 2 and 3). After 1 day at 120 ° $PhMeSiH_2$ gave full conversion but only 53% conversion. Whereas Et_3SiH gave trace conversion and yield at 120 ºC after 1 d. Next polymethylhydrosiloxane was tested (Entry 4) due to it being a stable, inexpensive, and non-toxic silane. However, poor conversion and trace yields were seen when reacted with acetone. Similar results to PMHS were seen when 1,1,3,3-

tetramethyldisilazane (TMDS) was used as the silane (Entry 6). Triethoxysilane is a tertiary silane that gave good results in past publications.[9g,h] This gave full conversion and a good yield of 71% which are similar results to entry 1 in Table 4.

Table 4. Testing of various silanes for the reduction of acetone to 2-propanol. [a] Yields were calculated using ^{1}H-NMR.

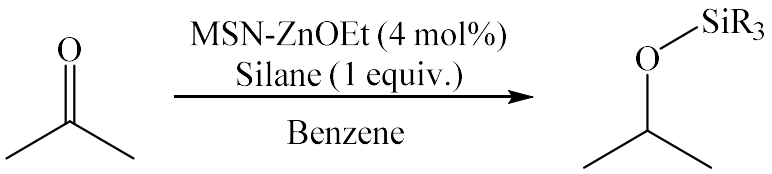

Entry	Silane	Time	Temp (°C)	Conv. (%)	Yield[a] (%)
1	$PhSiH_3$	3 h	60	100	78
2	$PhMeSiH_2$	1 d	120	100	53
3	Et_3SiH	1 d	120	Trace	Trace
4	PMHS	3 h	80	57	Trace
5	$(EtO)_3SiH$	3 h	60	100	71
6	TMDS	1 d	80	100	29

Next, the scope and limitations of the MSN-ZnOEt pre-catalyst were determined (Table 5). For these reactions 4 mol% of zinc pre-catalyst and 1.1 equivalent of silane was used while being heated between 60-80 ºC for 1 h – 1 d. Good yields were obtained when diaryl ketones were involved (Table 5 entries 7-10). The yields went down slightly, but were still decent, when dealing with aliphatic ketones (Table 5 entries 1-3 and 11-12). When hydrosilylating benzaldehyde the conversion was very quick with 1 h and gave good yield of 87% and 79% (Table 5 entries 13 and 14 respectively). When testing α,β-unsaturated ketones, chalcone in this case, the carbonyl was reduced and the olefin was left alone (Table 5 entry 14 and 15). Ester cleavage was seen when methylbenzoate was used and produced benzyl alcohol (Table 5 Entry 17). However, when CO_2 was tested no reaction was seen and $PhSiH_3$ was still present in the ^{1}H NMR (Table 5 entry 18).

Table 5. Catalytic reduction of various carbonyl containing compounds using 4 mol % catalyst. [a] Yields were calculated using ^{1}H-NMR.

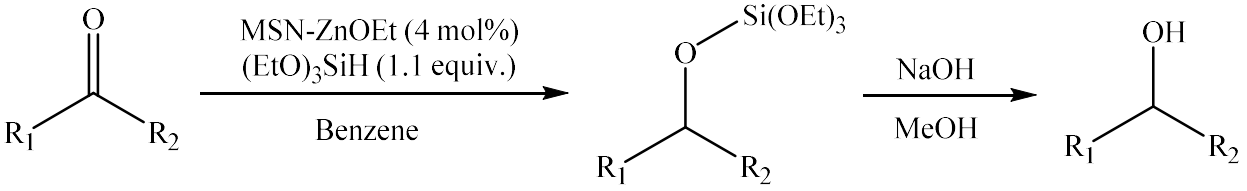

Entry	Ketone	Silane	Time	Temp (°C)	Conv. (%)	Yield[a] (%)	Product
1	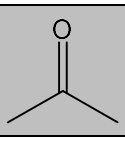	$PhSiH_3$	1 d	r.t.	100	78	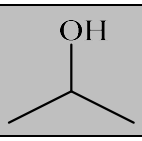
2		$PhSiH_3$	3 h	60	100	65	
3		$(EtO)_3SiH$	3 h	60	100	71	
4	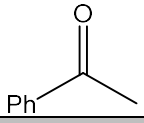	$PhSiH_3$	3h	80	100	36	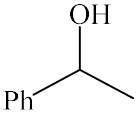
5		$(EtO)_3SiH$	4 h	80	95	77	
6	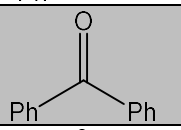	$PhSiH_3$	3 h	80	97	80	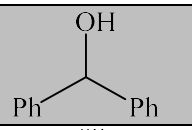
7		$(EtO)_3SiH$	3 h	80	100	81	
8	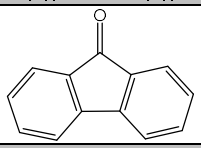	$PhSiH_3$	3 ½ h	80	100	89	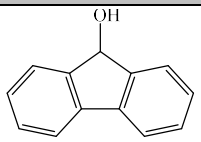
9		$(EtO)_3SiH$	2 h	80	100	95	
10	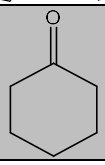	$PhSiH_3$	2 h	80	100	62	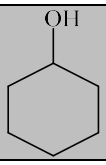
11		$(EtO)_3SiH$	1 h	80	100	78	
12	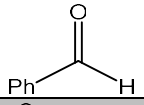	$PhSiH_3$	3 h	60	100	87	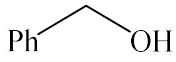
13		$(EtO)_3SiH$	1 h	60	100	79	
14	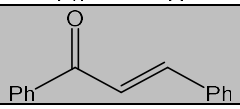	$PhSiH_3$	1 h	80	91	25	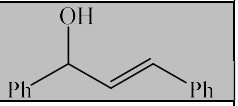
15		$(EtO)_3SiH$	3 h	60	83	13	
16	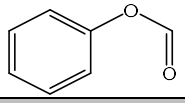	$PhSiH_3$	20 h	80	-	-	-
17	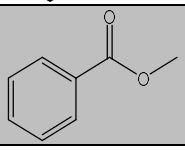	$PhSiH_3$	3 h	60	100	-	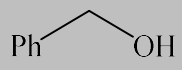
18	CO_2	$PhSiH_3$	1 d	60	-	-	-

It has been shown that the MSN-ZnOEt catalytic system is active for the heterogeneous hydrosilylation of carbonyl containing compounds. We then wanted to expand this system and

find new catalytic reactions it was active for. Zinc is well known to be active for the epoxidation of α,β-unsaturated ketones.[19] It was decided then that we will try out our system for the heterogeneous epoxidation of enones.

As stated before it was known that the addition of $ZnEt_2$ to MSN would result in zinc ethyl being bound to the surface of MSN (MSN-ZnEt) and then react with an alcohol to give the MSN zinc alkoxy complex. Lewiński and coworkers showed that a reaction of *tert*-butyl hydroperoxide with a β-diketiminate ZnO^{t}Bu complex would result in the zinc alkylperoxide.[19e] This zinc peroxide would then go on to catalyze the epoxidation of chalcone (Scheme 7).

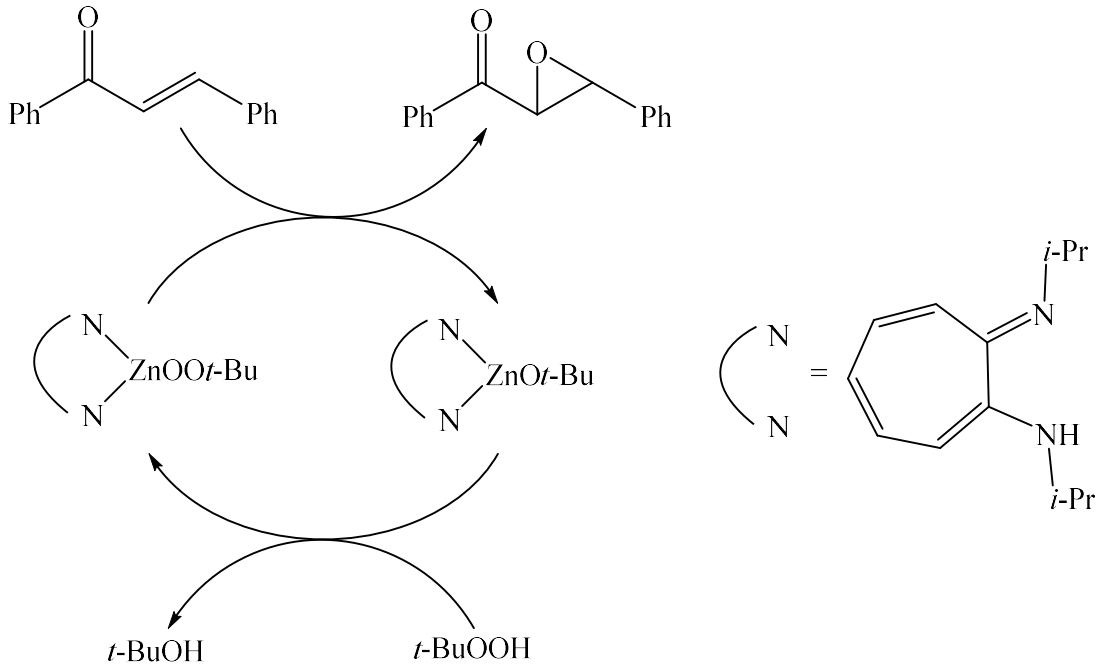

Scheme 7 Proposed catalytic cycle for the epoxidation of chalcone mediated by zinc alklperoxide/tert-BuOOH systems

By looking at Figure it can be seen that if you replace the β-diketiminate ligand with MSN it would fit well into what we have already shown we can do. We decide to use this reaction then and test wither MSN-ZnOEt would react with *tert*-butyl hydroperoxide to result in the

immobilization of an alkylperoxy zinc on the surface of MSN (MSN-ZnOO^{t}Bu). This in fact was the case (Scheme 8).

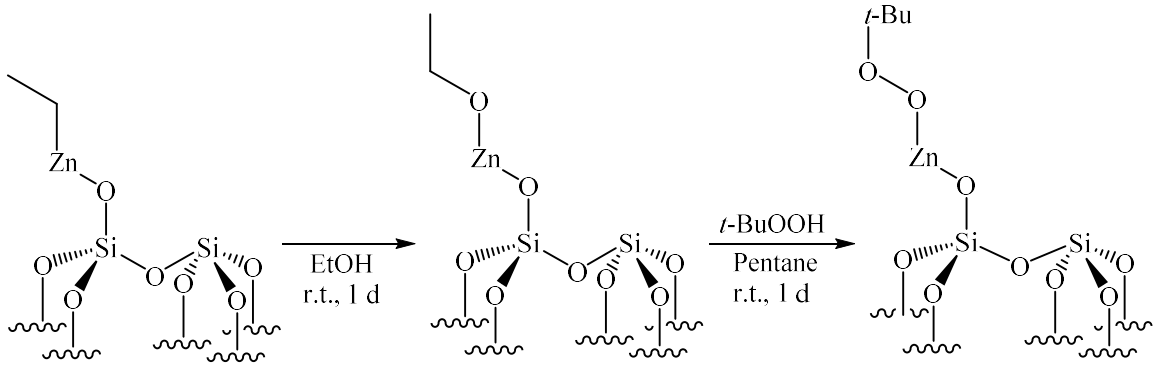

Scheme 8. Synthesis of ZnOO^{t}Bu on the surface of MSN

A simple reaction of the MSN-ZnOO^{t}Bu and triphenylphosphine was used to prove there was in fact a peroxide on the surface of MSN (Scheme 9). To make sure no tert-butyl hydroperoxide was left in the sample several washes with pentane were done and then the sample was dried overnight under reduced pressure. This reaction resulted in a peak at 24.64 ppm in the ^{31}P NMR indicating the formation of O=PPh$_3$ and the presence of a peroxide.

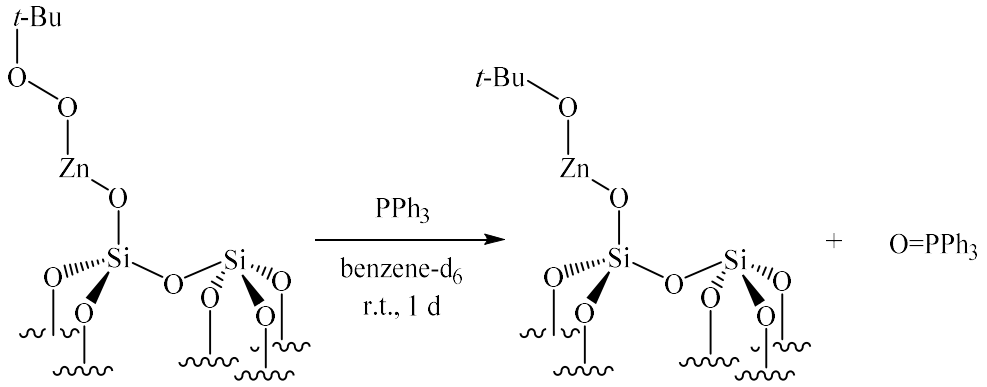

Scheme 9. Reaction of MSN-ZnOO^{t}Bu and PPh$_3$ to determine the presence of a peroxide

Once the peroxide was discovered to be on the surface, the catalytic activity of the catalyst system needed to be tested (Table 6). The enone chosen to test was trans-chalcone, which is known to be a reactive olefin towards epoxidation.[19] The peroxide used for this epoxidation was

tert-butyl hydroperoxide. The catalyst loading was 10 mol% and slight excess of peroxide at 1.2 equivalents. The background reaction of un-functionalized MSN was unsuccessful in the catalytic epoxidation by showing no conversion of *tert*-butyl hydroperoxide in the ^{1}H NMR. MSN-ZnEt and MSN-ZnOEt showed similar reactivity giving 58 and 59 percent conversion respectively. Though the reaction is slow and the yields are low, the system shows catalytic activity and now requires optimization.

Table 6. Catalytic testing of the epoxidation of *trans*-chalcone with *tert*-butylhydroperoxide. [a] Yields calculated using ^{1}H NMR

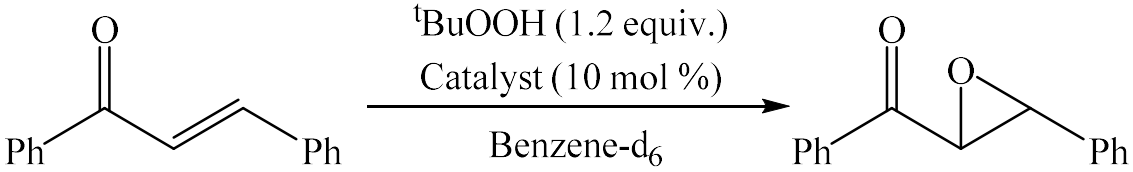

Pre-Catalyst	Peroxide	Time	Temp (°C)	Conv. (%)	Yield[a] (%)
MSN-ZnEt	^{t}BuOOH	1 d	60	58	36
MSN-ZnOEt	^{t}BuOOH	1 d	60	59	49
MSN	^{t}BuOOH	1 d	60	-	-

Conclusion

In conclusion, we have successfully synthesized the first heterogeneous zinc catalyst for the hydrosilylation of carbonyl-containing compounds. This novel system is easily produced by reacting $ZnEt_2$ with MSN at room temperature followed up by suspending the MSN-ZnEt in an alcoholic solvent to produce the desired zinc alkoxide. The zinc on the surface of MSN is homogeneously dispersed on the surface and in the pores providing multiple catalytic sites due to the high surface area of MSN. This pre-catalyst was shown to be efficient in reducing ketones to the corresponding alcohols and showed promising results in the reduction of aldehydes, esters and enones. It was found this system works well with $(EtO)_3SiH$ and $PhSiH_3$ as the reducing

agents and showing little to no reactivity with secondary or tertiary alkyl silanes. Further work is being done to extend the scope of this system by seeing how different functional groups are tolerated. This same system was then expanded to the epoxidation of α,β-unsaturated ketones with *tert*-butyl hydroperoxide. Decent conversion was seen with chalcone and could show greater results with optimization. It is believed that the first zinc alkyl peroxide has been isolated on the surface of MSN and is stable at room temperature.

This system shows great flexibility in catalyzing multiple reactions and good stability when it comes to temperature, air, and moisture. For future work the possible catalytic activity of this system will be expanded to the formation of secondary amines by coupling of aldehydes and amines in the presence of silanes and also for the reduction of amides to amines using silanes as the reducing agent.

Experimental

SBA- 15 Mesoporous Silicon Nanoparticles (MSN) synthesis by Sebastian Manzano in the Slowing research group This material was prepared following their previously reported method.[20] In a typical synthesis the triblock copolymer (Pluronic P104; 7.0 g) was dissolved in a mixture of 4M HCl aqueous solution (109.0 g) and deionized water (164.0 g, 18 megaohms) at 52 °C. Tetramethyl orthosilicate (TMOS; 10.6 g, 69.6 mmol) was quickly added into the solution and after continuous stirring for 24 h, the reaction mixture was then transferred into a teflon-lined high-pressure autoclave for further hydrothermal treatment at 150 °C for 24 h. The resulting white solid (SBA-15-type MSN product) was isolated by filtration, washed with copious amounts of water and methanol, and air-dried at 80 °C. Finally, the removal of the pluronic P104 surfactant was accomplished by calcination at 550 °C for 6 h.

MSN-ZnEt MSN (1.00 g, 1.93 mmol Si-OH/g) was suspended in pentane (10 mL) in a vial in the glovebox. Diethyl zinc (0.320 mL, 3.00 mmol) was added dropwise to the suspension. The mixture was stirred at room temperature for 1 d. To isolate the product, the vial was centrifuged, and the solvent was removed by pipet. The solid was washed with pentane (3x) and was dried under reduced pressure to give the product as a white powder solid (1.08 g, 0.866 mmol Zn/g, 91%). IR (KBr, cm^{-1}) 2956 w, 2869 w, 1088 s, 808 m.

MSN-ZnOEt MSN-ZnEt (1.00 g, 0.866 mmol Zn/g) was added to a vial in the glovebox. The solid was suspended in ethanol and let stir at room temperature for 1 d. To isolate the product, the vial was centrifuged, and the solvent was removed by pipet. The solid was washed with pentane (3x) and was dried under reduced pressure to give the product as a white powder solid (0.998 g, 0.847 mmol Zn/g, 98%) IR (KBr, cm^{-1}) 2973 w, 2924 w, 1088 s, 808 m.

MSN-ZnO^{t}Bu MSN-ZnEt (1.0 g, 0.8656 mmol Zn/g) was added to a vial in the glovebox. The solid was suspended in *tert*-butanol and let stir at room temperature for 1 d. To isolate the product, the vial was centrifuged, and the solvent was removed by pipet. The solid was washed with pentane (3x) and was dried under reduced pressure to give the product as a white powder solid (1.00 g, 0.7296 mmol Zn/g, 97%). IR (KBr, cm^{-1}) 2976 w, 2927 w, 1101 s, 815 m

MSN-Zn nanoparticles MSN-ZnEt (0.020 g, 0.017 mmol Zn/g) was added to a J. Young NMR tube. Benzene was then added followed by phenyl silane (0.004 mL, 0.034 mmol). This mixture was then heated to 80 °C for 1 hour. The white solid becomes black and settles on the bottom.

General procedure for NMR scale hydrosilylations To a J. Young NMR tube MSN-[Zn] (4.00 mol %) was added. MSN-[Zn] was suspended in deuterated solvent (0.500 mL). To the mixture hexamethylbenzene standard (0.030 mL, 0.006 mmol, 0.2M solution) was added. Silane was

added (0.144 mmol) to the mixture followed by the carbonyl containing compound (0.120 mmol). The mixture was then heated to 60 – 80 °C for 1 – 3 hours depending on the compound. ^{1}H NMR (600 MHz, benzene-d_6)

MSN-ZnOO^{t}Bu MSN-ZnEt (0.100g, 0.0866 mmol) was suspended in pentane (10 mL) in a vial in the glovebox. Tert-Butyl hydroperoxide (0.0545 mL, 0.300 mmol, 5.5M in decane) was added to the vial and the mixture was stirred for 1 d at room temperature. To isolate the product, the vial was centrifuged, and the solvent was removed by pipet. The solid was washed with pentane (3x) and was dried under reduced pressure to give the product as a white powder solid (0.098 g, 93%).

Reaction of MSN-ZnOO^{t}Bu with triphenylphosphine MSN-ZnOO^{t}Bu (0.010g, 0.0087 mmol) was added to a J. Young Tube. In a test tube triphenylphosphine (0.005g, 0.018 mmol) was dissolved in Benzene-d_6. The triphenylphosphine solution was added to the MSN-ZnOO^{t}Bu at room temperature. The mixture was shaken for 1 day at room temperature. ^{31}P NMR (243.04 MHz, benzene-d_6) 24.64 ($O{=}PPh_3$).

Epoxidation of Chalcone To a J. Young tube MSN-ZnEt or MSN-ZnOEt (0.005 g, 0.0043 mmol Zn) was added. Benzene-d_6 (0.5 mL) was added. Chalcone (0.009g, 0.045 mmol) was added. Then hexamethylbenzene (0.030 mL, 0.06 mmol) was added as the standard. Lastly *tert*-butyl hydroperoxide (0.023 mL, 0.054 mmol) was added. The J. Young tube was sealed and the mixture was heated for 1 day at 80 °C. 59 % yield. ^{1}H NMR (600 MHz, benzene-d_6)

Material Characterization Small angle X-ray diffraction pattern (XRD) was performed on a Bruker AXS D8 Discover instrument operated at 40 kW using CuαK radiation. The nitrogen sorption isotherms were measured at liquid nitrogen temperature using a Micromeitics ASAP 3000 analyzer. The Brunauer-Emmett-Tell (BET) model was used to calculate the apparent surface area

and pore volume, and the pore size distribution was calculated by the Barrett-Joyner-Halenda (BJH) method. Transmission Electron Microscopy (TEM) images were obtained using a FEI Tecnai G2 F20 working at 200 kV. TEM samples were prepared by placing 2-3 drops of dilute methanol suspensions onto a carbon-coated copper grid.

Zn loadings were analyzed in a Perkin-Elmer Optima 2100 DV inductively coupled plasma-optical emission spectroscope (ICP-OES). Samples (3 mg) were digested for 16 hours in aqueous HF solution (10 v/v %).

References

1. Aroop K. Roy* *Advances in Organometallic Chemistry*, **2007**, *55*, 1-59
2. Reuben G. Jones and Edmund C. Kornfeld *J. Am. Chem. Soc*. **1951**, *73*, 107-109
3. Fumio Toda*, Koji Kiyoshige, and Minoru Yagi *Angew. Chem. Int. Ed. Engl*. **1989**, *28*, 320-321
4. Examples of Rh hydrosilylation a.) Hisao Nishiyama*, Hisao Sakaguchi, Takashi Nakamura, Mihoko Horlhata, Manabu Kondo, and Kenji Itoh. *Organometallics* **1989**, *8*, 846-848. b.) Masaya Sawamura, Ryoichi Kuwano, and Yoshihiko Ito* *Angew. Chem. Int. Ed. Engl*. **1994**, *33*, No. 1, 111-113. c.) Beata Tao and Gregory C. Fu* *Angew. Chem.* **2002**, *114*, No. 20, 4048-4050. d.) Vincent César, Stéphane Bellemin-Laponnaz* and Lutz H. Gade* *Angew. Chem.* **2004**, *116*, 1036-1039.
5. Examples of Ru hydrosilylation a.) Yoshiaki Nishibayashi, Izuru Takei, Sakae Uemura,* and Masanobu Hidai* *Organometallics* **1998**, *17*, 3420-3422. b.) Guoxin Zhu, Michael Terry, Xumu Zhang* *Journal of Organometallic Chemistry* **1997**, *547*, 97-101. c.) Ian C.

Lennon and James A. Ramsden* *Organic Process Research & Development* **2005**, *9*, 110-112.

6. Examples of Ir hydrosilylation a.) Annegret Kinting, Hans-Jörn Kreuzfeld* *Journal of Organometallic Chemistry*, **1989**, *370*, 343-349. b.) J.W. Faller* and Kevin J. Chase *Organometallics,* **1994**, *13*, 989-992. c.) Anthony R. Chianese and Robert H. Crabtree* *Organometallics*, **2005**, *24*, 4432-4436.
7. Example of Ti hydrosilylation Jasesook Yun and Stephen L. Buchwald* *J. Am. Chem. Soc*. **1999**, *121*, 5640-5644.
8. Examples of Cu hydrosilylation a.) Dong-won Lee and Jaesook Yun* *Tetrahedron Letters* **2004**, *45*, 5415-5417. b.) Sabine Sirol, James Courmarcel, Naouël Mostefai, and Olivier Riant* *Organic Letters*, **2001**, *3*, 4111-4113. c.) Bruce H. Lipshutz,* Asher Lower, and Kevin Noson *Organic Letters*, **2002**, *4*, 4045-4048. d.) Bruce H. Lipshutz,* Kevin Noson, Will Chrisman, and Asher Lower *J. Am. Chem. Soc***. 2003**, *125*, 8779-8789. e.) Nicholas J. Lawrence* and Simon M. Bushell *Tetrahedron Letters*, **2000**, *4*, 4507-4512. f.) Jean Thomas Issenhuth, Samuel Dagorne,* and Stéphane Bellemin-Laponnaz *Adv. Synth. Catal*. **2006**, *348*, 1991-1994.
9. Example of Zn hydrosilylation a.) Hubert Mimoun. *J. Org. Chem*. **1999**, *64*, 2582-2589 b.) Hubert Mimoun,* Jeasn Yves de Saint Laumer, Luca Giannnini, Rosario Scopelliti, and Carlo Floriani *J. Am. Chem. Soc*. **1999**, *121*, 6158-6166. c.) Virginie Bette, André Mortreux,* Federico Ferioli, Gianluca Martelli, Diego Savoia,* and Jean-François Carpentier* *Eur. J. Org. Chem*. **2004**, 3040-3045. d.) Virginie Bette, André Mortreux, Diego Savoia, and Jean-François Carpentier* *Tetrahedron* **2004**, *60*, 2837-2842. e.) Virginie Bette, André Mortreux,* Diego Savoia, Jean-François Carpentier* *Adv. Synth.*

Catal. **2005**, *347*, 289-302. f.) Jadwiga Gajewy, Marcin Kwit,* and Jacek Gawroński* *Adv. Synth. Catal*. **2009**, *351*, 1055-1063. g.) Stephan Enthaler,* Björn Eckhardt, Shigeyoshi Inoue, Elisabeth Irran, and Matthias Driess *Chem. Asian J*. **2010,** *5*, 2027-2035. h.) Shuai Liu, Jiajian Peng,* Hu Yang, Ying Bai, Jiayun Li, Guoqiao Lai* *Tetrahedron* **2012**, *68*, 1371-1375. i.) Wesley Sattler and Gerard Parkin* *J. Am. Chem. Soc*. **2012**, *134*, 17462-17465.

10. Examples of heterogeneous Rh hydrosilylation a.) Jun-ichi Ishiyama,* Yasuhisa Senda, Isamu Shinoda, and Shin Imaizumi *Bulletin of the Chemical Society of Japan*, **1979**, *52*, 2353-2355. b.) Guillermo Lázaro, Francisco J. Fernández-Alvarez,* Manuel Iglesias, Cristina Horna, Eugenio Vispe, Rodrigo Sancho, Fernando J. Lahoz, Marta Iglesias, Jesús J. Pérez-Torrente and Luis A. Oro* *Catal. Sci. Technol*. **2014**, *4*, 62-70. c.) Guillermo Lázaro, Francisco J. Fernández-Alvarez,* Julen Munárriz, Victor Polo, Manuel Iglesias, Jesús J. Pérez-Torrente and Luis A. Oro* *Catal. Sci. Technol*. **2015**, *5*, 1878-1887.
11. Q.-H. Xia H.-Q. Ge, C.-P. Ye, Z.-M. Liu, and K.-X. Su *Chem. Rev*. **2005**, *105*, 1603-1662
12. Tsutomu Katsuki and K. Barry Sharpless *J. Am. Chem. Soc*. **1980**, *102*, 5974-5976
13. Sankaranarayanapillai Shylesh, Mingjun Jia, and Werner R. Thiel* *Eur. J. Inorg. Chem*. **2010**, 4395-4410.
14. Dieter Enders*, Jiqun Zhu, and Gerhard Raabe. *Angew. Chem. Int. Ed. Engl*. **1996**, *35*, 1725-1728
15. Haiming Wang, Zheng Wang, Kuiling Ding*. *Tetrahedron Lett.* **2009**, *50*, 2200-2203

16. Christophe Copéret,* Mathieu Chabanas, Romain Petroff Saint-Arroman, and Jean-Marie Basset*. *Anew. Chem. Int. Ed*. **2003**, *42*, 156-181

17. Kyle L. Fujdala and T. Don Tilley* *J. Am. Chem. Soc*. **2001**, *123*, 10133-10134

18. Debabrata Mukherjee, Richard R. Thompson, Arkady Ellern, and Aaron D. Sadow* *ACS Catal*. **2011**, *1*, 698-702

19. a.) Hong-Bin Yu, Xiao-Fan Zheng, Zhi-Ming Lin, Qia-Sheng Hu, Wei-Sheng Huang, and Lin Pu* *J. Org. Chem*. **1999**, *64*, 8149-8155. b.) Michael J. Porter and John Skidmore *Chem. Commun*. **2000**, 1215-1225. c.) Janusz Lewiński,* bigniew Ochal, Emil Bojarski, Ewa Tratkiewicz, and Iwona Justyniak *Angew. Chem. Int. Ed*. **2003**, *42*, 4643-4646. d.) Benjamin S. Lane and Kevin Burgess* *Chem. Rev*. **2003**, *103*, 2457-2473. e.) Marcin Kubisiak, Karolina Zelga, Iwona Justyniak, Ewa Tratkiewicz, Tomasz Pietrzak, Abdul R. Keeri, Zbigniew Ochal, Larissa Hartenstein, Peter W. Roesky, and Janusz Lewiński* *Organometallics*, **2013**, *32*, 5263-5265. f.) Takayoshi Hara, Jun Kurihara, Nobuyuki Ichikuni and Shogo Shimazu* *Catal. Sci. Technol*. **2015**, *5*, 578-583.

20. Kim, T.-W.; Slowing, I. I.; Chung, P.-W.; Lin, V. S.-Y. *ACS Nano*. **2010**, *5*, 360−366.

CHAPTER 3

DESIGN, TESTING, AND USE IN CATALYSIS OF 3D PRINTED STRUCTURES CONTAINING A TRANSITION METAL CATALYST

Jacob Fleckenstein, Sebastián Manzano, Zak Weinstein, Igor I. Slowing*, and Aaron D. Sadow*

Department of Chemistry, U.S. DOE Ames Laboratory, Iowa State University, Ames, IA 50011-3111

Abstract

Stereolithography (SLA) three-dimensional (3D) printing photopolymerizes acrylic resin into a solid polymer. By use of the Formlabs software (Preform) 3D drawings are broken down into slices which allows for the drawing to be printed layer by layer. Using this method a Pd/C and acrylic resin were mixed and printed into a solid 3D object. This palladium-polymer composite was analyzed using chemisorption, and ICP-MS which showed there was exposed palladium on the surface of the 3D printed object. Unique designs were implemented to allow the catalyst to be inserted into a reaction, be easily removed, and to allow hydrogen gas to be flowed into the reaction for the reduction of functional groups using palladium. The 3D printed catalyst partially converted benzaldehyde to benzyl alcohol and toluene.

§ Other authors' contributions

Sebastián Manzano: Surface characterization of 3D printed objects, collaboration on designs and reactions with 3D printed objects

Zak Weinstein: Collaboration on designs and reactions with 3D printed objects

Igor I. Slowing: Collaboration on designs and reactions with 3D printed objects

Introduction

3D printing is the ultimate technology for the customization of 3D objects. The only limit is the imagination of the designer and their ability to design an object in a 3D drawing software. This technology can be expanded in unlimited ways in the chemical world limited by the materials being printed and the 3D printer itself. These examples include adding carbon nanotubes to photo-curable resins,[1] low-cost conductive composite material for 3D printing of electronic sensors,[2] solid freeform fabrication of stainless steel,[3] 3D printed quantum dot light-emitting diodes,[4] and 3D printed millifluidic and microfluidic 'lab on a chip' reactionware devices.[5] An example of this is the ability to 3D print custom reactionware that can incorporate analytical instruments into the reaction vessel or reactionware suited for a specific reaction. These examples are highly sought after due to the high cost and expertise it takes to make the specific glassware required. The different reported examples of printed reactionware include a print where the formation of the inorganic nanoclusters can be observed by a camera (Figure 1),[6] a three step reaction where each step is

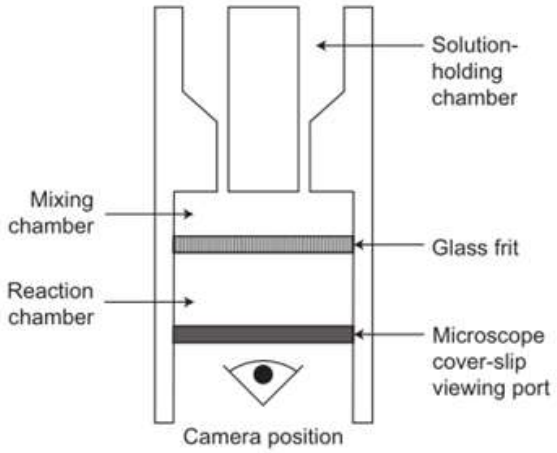

Figure 1 3D printed reactor in which the reaction can be observed by a camera

taking place in a different section of the reactor (Figure 2),[7] a multi-well block that is able to

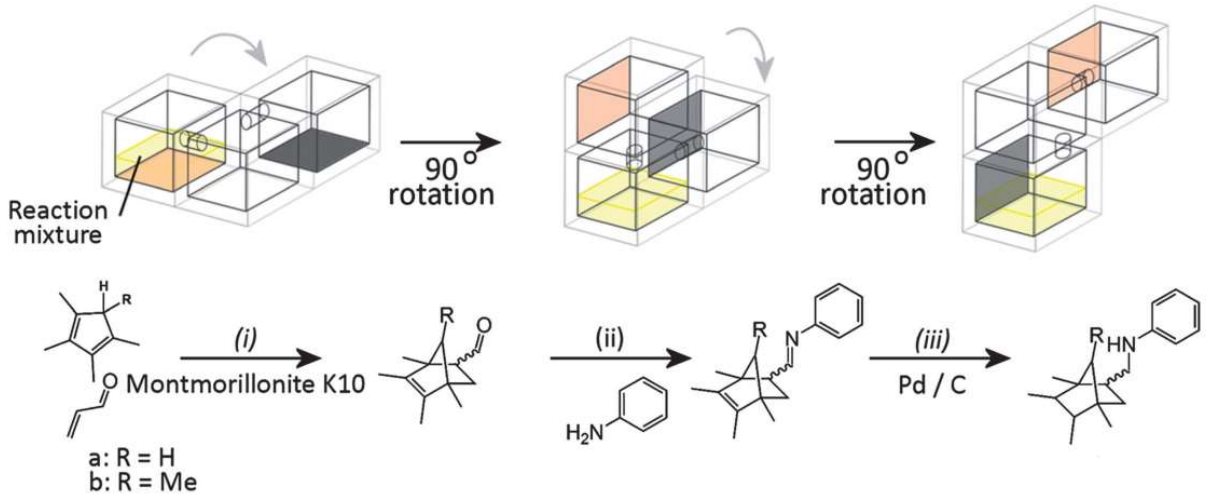

Figure 2 3D printed reactor where each section is a different reaction for a multistep synthesis withstand pressure suited for high-throughput screening of the formation of molecular organic frameworks (Figure 3),[8] a flow reactor that was attached to an infrared spectrometer analyzing

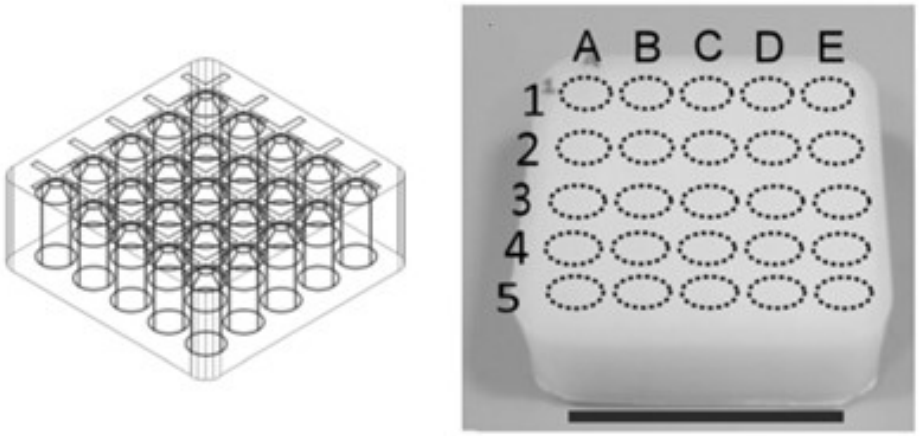

Figure 3 3D printed high pressure reactor

the formation of imines from the reaction of aldehydes and amines (Figure 4),[9] and a device capable of studying drug transport and cell viability (Figure 5).[10] Although the reactions in these examples are known, the interesting aspect is the way 3D printing technology was applied to make unique reactors. 3D printing allows for the production of complicated reactors that would otherwise require expensive and hard to make glassware.

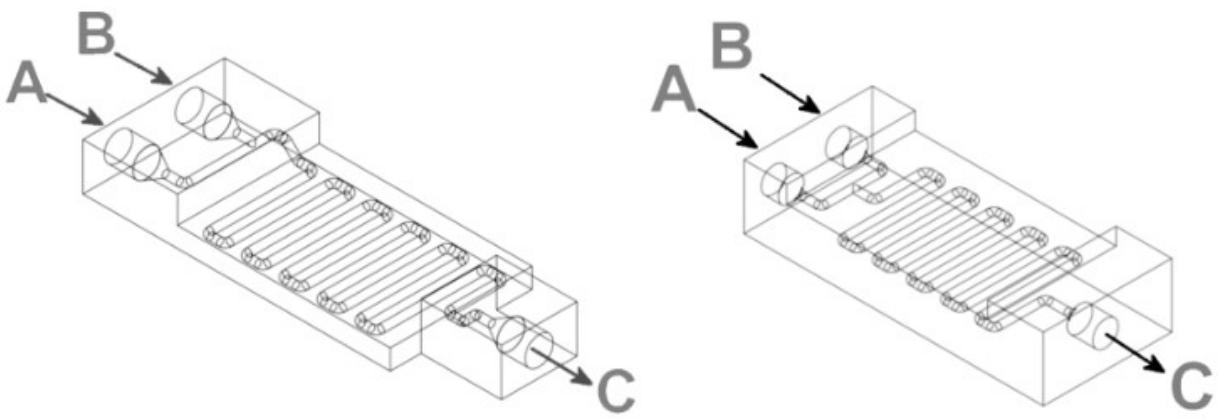

Figure 4 3D printed flow reactor for the formation of imines

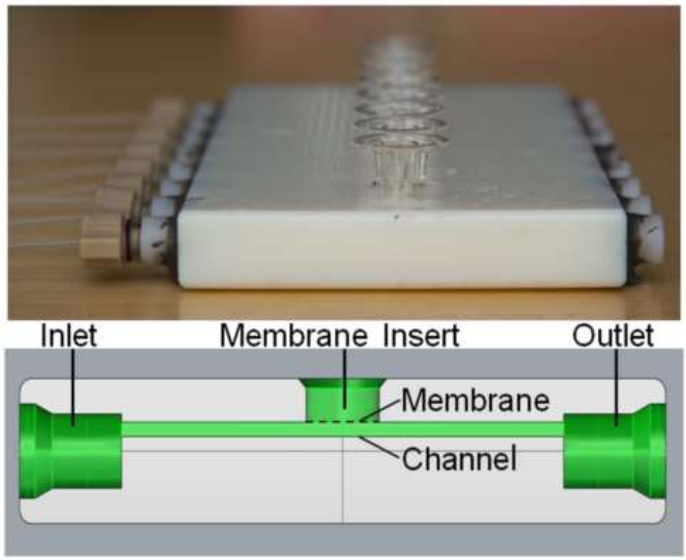

Figure 5 3D printed reaction vessel capable of study drug transport

Another way to utilize 3D printing technology in the chemical world would be the ability to 3D print catalysts into specific shapes that could be incorporated into organic synthesis. This ability could lead to the next breakthrough in heterogeneous catalysis such as a 3D printed flow reactor whose walls are lined with a catalyst. Being able to print your catalyst as an insert to a reaction, the reaction vessel itself or combine multiple catalysts into a single print by using multiple "catalytic" filaments would also be an extremely powerful tool in heterogeneous catalysis.

Herein we demonstrate the common and important catalyst “Pd/C” can be manipulated in a 3D printer resulting in a 3D printed object containing a transition metal catalyst. This 3D printed catalyst was then tested for the catalytic reduction of a nitro group to an amine under a hydrogen atmosphere and the reduction of benzaldehyde to benzyl alcohol. Also, a 3D printed reactor that can withstand multiple organic solvents and a pressure up to 5 bar of hydrogen was designed and printed. Described below is a unique design to incorporate the 3D printed catalyst into a reaction. The value of 3D printed catalysts has been demonstrated by the ease in which the catalyst can be removed from the reaction, the catalysts ability to be recycled and the ability to create specific shapes that can be designed for a specific use or reaction. In addition, this design can be expanded to test multiple 3D catalyst shapes at one time under the same environment.

Results and Discussion

The initial idea was to use a simple known reaction to test with a 3D printed catalyst. The catalyst to be used would be the well-known and well tested Pd/C catalyst for the reduction of functional groups with hydrogen. Two example reactions we wanted to try were the reduction of alkynes to alkanes and also the reduction of nitro groups to amines (Scheme 1).

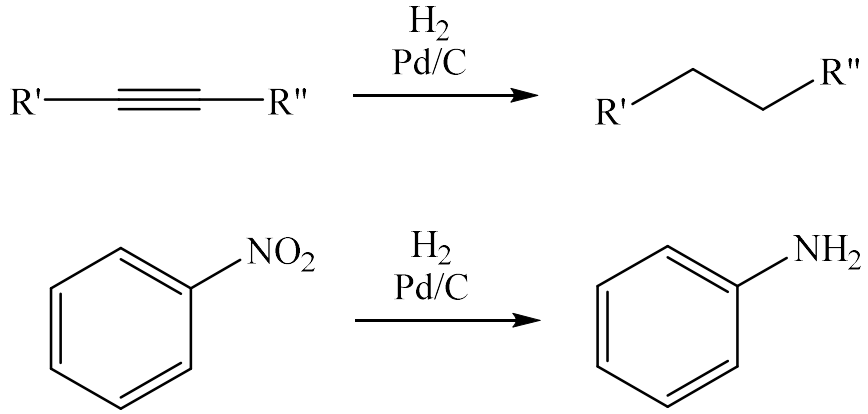

Scheme 1 Example of test reactions for 3D printed catalyst

Once the catalyst was decided upon the design for the 3D printed catalyst needed to be made. First we wanted to see if the SLA printer would still print simple shapes with Pd/C mixed in with the photo active resin. We then mixed in 350 mg of 10 wt% Pd/C into 150 mL of clear resin bought from Formlabs and printed spheres (Figure 6). Once we knew that the mixture allow for the polymerization to proceed we went about design the catalyst shapes to be used.

Figure 6 3D printed spheres containing Pd/C.

Four catalyst cap ends were designed, using the AutoCAD software, to have the most surface area possible and still be strong enough structurally to be able to be printed and reused (Figure 7). It was believed the design with the most surface area would increase the rate of the reaction. This could also be used to test how different shapes affect the reaction in certain ways such as rate or conversion. This aspect is where 3D printing is key due to the ability to change the design to suit your needs and then print it.

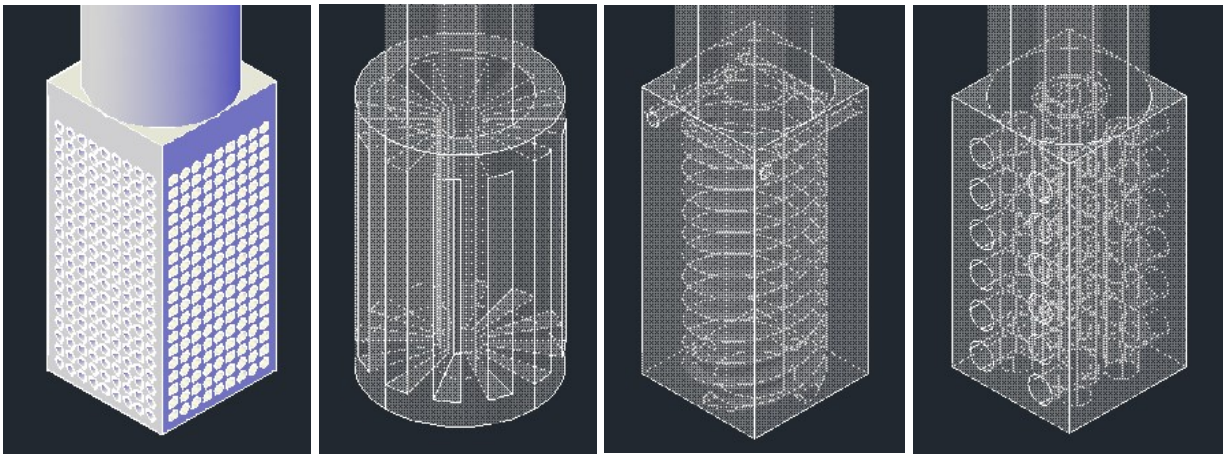

a b c d

Figure 7. 3D drawings using the Autodesk Autocad 2014 software. (a) Porous box (Conceptual view). Surface area = 4769 mm^2. 0.75 mm in diameter pores that go through the x and z axis. A 4 mm pore travels through the center allowing hydrogen gas to flow. (b) Pinwheel (X-ray view). Surface area = 3433 mm^2. Pores 18 mm long and 2 mm wide surround the cylinder and travel to its core and open into the central pore. A 4 mm pore runs down the center to allow hydrogen flow. (c) Helical box (X-ray view). Surface area = 2331 mm^2. Four 1 mm pores trace a helix though the box circling a central pore that is 4 mm in diameter. Each pore is open on one side of the box and then again at the base. (d) Pillared Box (X-ray view). Surface area = 1715 mm^2. Four 2 mm in diameter pillars travel from the base up the box. Six 2 mm pores are connected to each pillar. A central 4 mm collumn travels the length of the box and also connects with the four other pillars.

Each design seen in Figure 7 was similar in size since the rectangular prism that the designs were subtracted from are the same length, height and width. The porous box design (Figure 7a) was by far the most surface area at 4769 mm^2 and was then predicted to have the most activity due to more Pd being acessible for the reaction. Increasing the diameter of the pores would increase the surface area, however, 0.75 mm pores were close to the limit of gaining porosity and losing strength in the structure. This was found by increasing the diameter of the pores and the prints failing. Also, by compairing the same 3D printed objects, the addition of Pd/C to the resin did not seem to affect the resolution. The helical design Figure 7-c was influenced by a flow reactor. The idea being that the reactants would be able to move through the helical pores and have a more extended exposure to the palladium on the surface of the catayst insert (CI).

As stated before, the idea was to have the ability to flow hydrogen into the reaction while still incorporating the catalyst which is where the design of an insert comes in (Figure 8). The CI has a channel running through the middle that allows the gas to enter inside the reaction vessel where there reaction is taking place. The CI is novel by itself due to the ability to screw in and out of the reactor vessel top. This is beneficial because you can remove the catalyst as you seen fit or replace it with a different metal catalyst to catalysze the next step in the reaction.

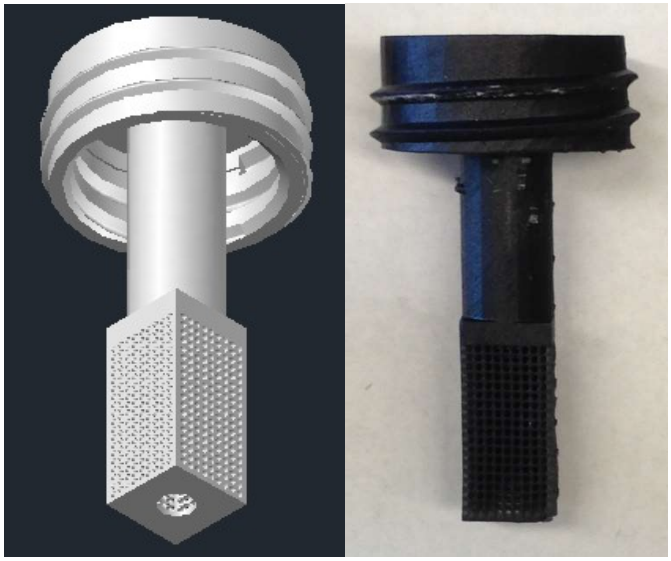

Figure 8 CI Porous Box. Left – CAD drawing. Right – 3D printed CI

As seen in Figure 8 the CI has a black color to it, which comes from the Pd/C contained within the print. The resin used for the 3D printing orginally is colorless so if no palladium was added the print would be transparant. The Pd/C was added directly to the resin tank that contained the clear resin. 350 mg 10 wt% Pd/C was added to 150 mL resin equaling out to 0.26 mg Pd per mL of resin. This mixture was then homogenized and used for printing. For scale, the end of the CI where the pores are is around 1 mL and the entire CI contains about 6 mL of resin, which is only 1.56 mg of Pd. Chemisorption experiments on 3D printed objects with Pd/C show that there is metal on the surface of the objects. Tests were run on three separate objects all

printed at the same time and the same shape. The results show a metallic surface area (m^2/g sample) of 0.022, 0.012, and 0.034 for the three different samples. This proves then there is exposed Pd on the surface of the object which should be catalytically active.

The next step was to design and print a reactor that will allow hydrogen to be flowed in and hold the pressure that gets built up. The design was influenced from a regular parr-bomb reactor. Since the PMMA polymer gets printed as a solid polymer, using the SLA type Formlabs 1+ printer, we felt that this was the best chance for the reactor to hold pressure. The main challenge was to be able to take apart the reactor in order to add reagents to the reaction or to remove the end product. This requirement meant a seal was needed. Another problem was the need to release pressure once it was built up. The designs for the reactor vessel and solutions to these problems can be seen in Figure 9 and 10. As you can see the arm on the side of the reaction vessel allows for the pressure to be released through a known direction.

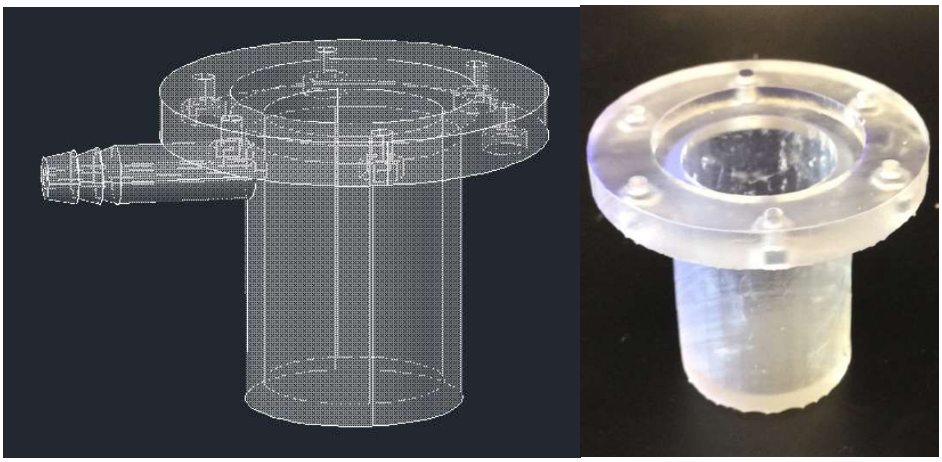

Figure 9 Reaction vessel bottom. Left – CAD design. Right – 3D printed object.

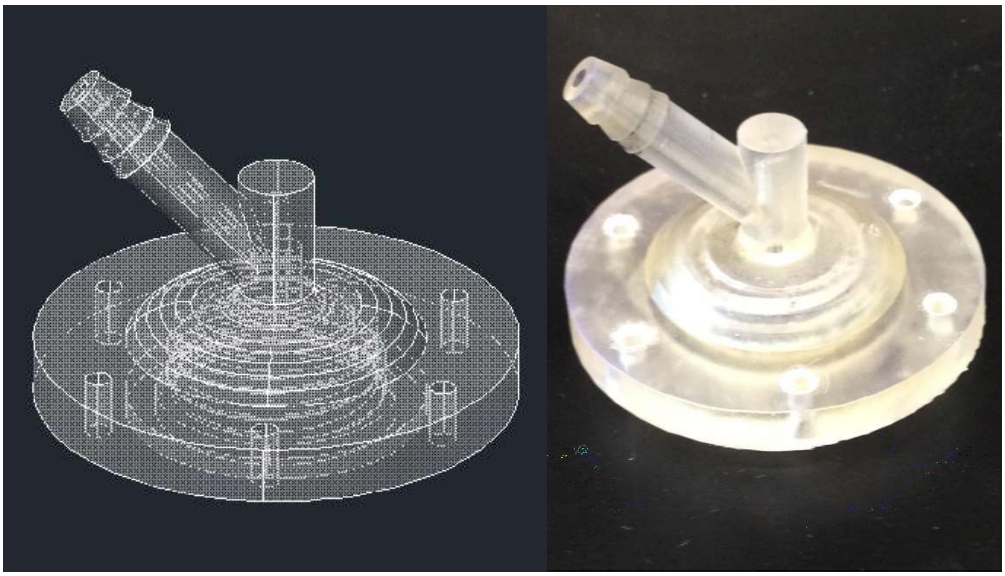

Figure 10 Reaction vessel top. Left – CAD design Right – 3D printed object.

For there to be a proper seal there is a place to fit a rubber gasket in the reaction vessel bottom (Figure 9). When the top gets screwed down it squeezes the rubber gasket making a gas tight seal (Figure 10). The reaction vessel top then has a section for the CI to be screwed into it. This is what holds the CI in place during the reaction and also allows the CI to be replaced without replacing the entire reactor. The top and bottom of the reaction vessel are then held together by 6 nuts and bolts. The bolts get held into place by hexagonal holes seen in Figure 3.

As stated before the pressure was needed to be able to be released once it was built up. This was accomplished by designing a screw valve that is able to release the pressure slowly by unscrewing the plunger and allow the hydrogen to flow out (Figure 11). This designed solved the problem of the pressure being released by unscrewing the top of the reaction vessel. Through use of the screw valve we were able control the release of pressure.

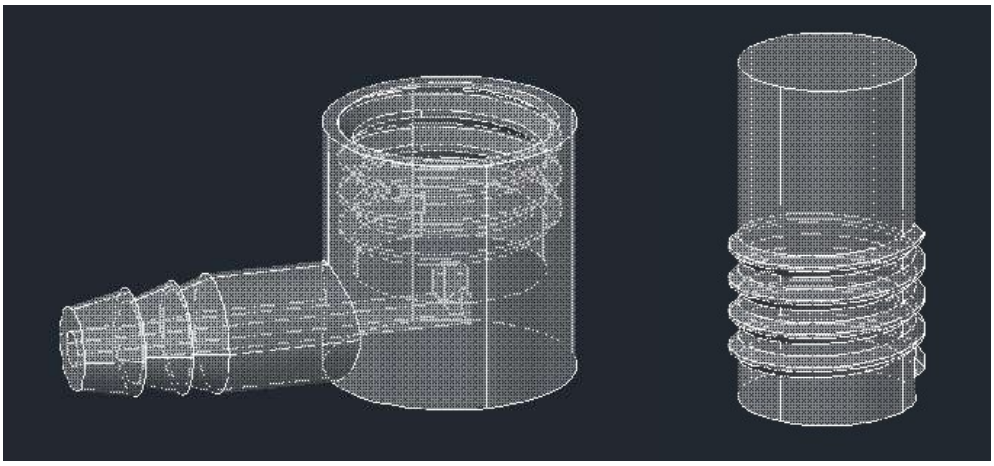

Figure 11 Screw valve CAD designs.

With this set up the entire system is able to be pressurized up to 5 bar and allowing the pressure to be released in a slow, steady, and safe manner.

Shown in Figure 12 is the complete set up. The hose coming in from the top is the hydrogen in line. The hydrogen then gets lead into the reaction vessel through the canal in the CI. The screws holding the top and bottom together can also been seen, however the rubber gasket can not been seen. The dark portion seen in the middle of the reaction vessel bottom is the CI that is attached to the top of the reaction vessel. The CI hangs down in the middle but still gives room for a stir bar at the bottom. The hose leading to the right of the picture is the pressure release hose which is attached to the pressure release valve.

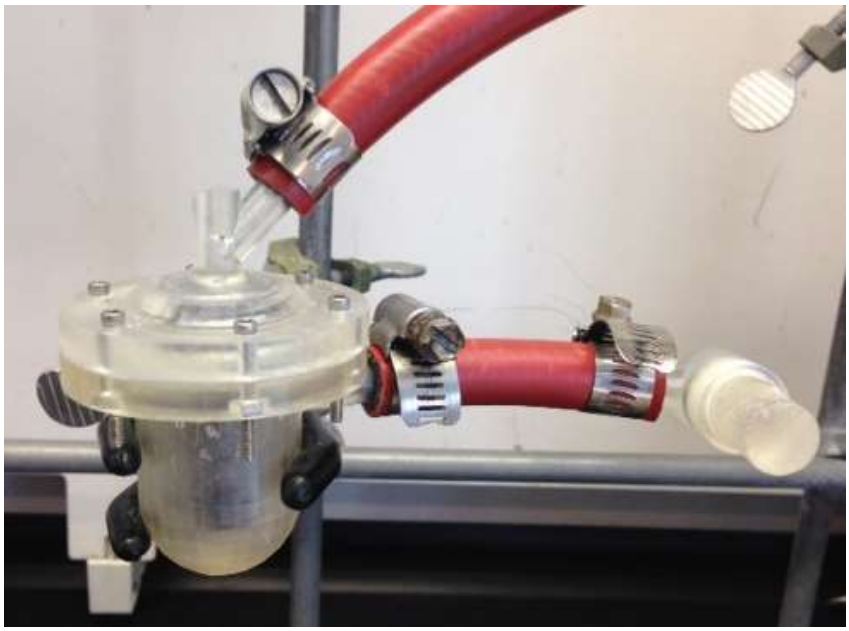

Figure 12 Complete 3D printed reaction vessel with CI.

Once the reactor and CI were designed and printed it was time to test the catalytic activity of these 3D printed catalysts. It is known that polymers are stable in some solvents and not in others. In order to test which solvents these 3D printed objects were stable in the CIs were let sit in various solvents (Table 1). It was found that the CIs degrade in majority of solvents, though there was a trend seen. The higher molecular weight of the alcoholic solvent the slower the CI degraded and then they were stable in butanol (Table 1 Entry 4). Hexanes was also found to be a solvent the CIs were stable in (Table 1 Entry 5).

Table 1 – Solvent testing of CIs

Entry	Solvent	Stability
1	Methanol	Degrades – 2 hr
2	Ethanol	Degrades – 6 hr
3	Isopropanol	Degrades – 1 d
4	Butanol	Stable
5	Hexanes	Stable
6	Benzene	Degrades – 1 d
7	THF	Degrades – 6 hr
8	Methylene Chloride	Degrades – 12 hr

Once two solvents were found not to degrade the CI it was time to try the catalysis. Using the 3D printed reaction vessel and a CI the reduction of nitrobenzene in butanol was tried under 5 bar of hydrogen (Scheme 2).

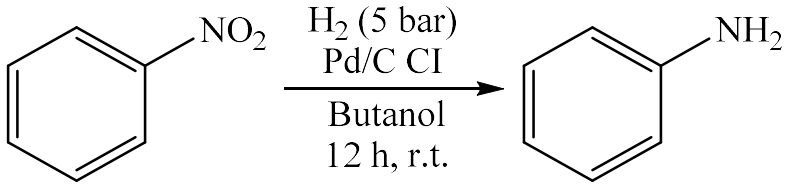

Scheme 2 Reduction of nitrobenzene to aniline in butanol using hydrogen and a 3D printed CI

After the 12 hours at room temperature the reaction was stopped and it was found that the CI did degrade during the reaction. However, analysis of the reaction using GC-MS did show the production of aniline. The reaction was then tried in hexanes (Scheme 3). After the 12 hours at room temperature it was found that the CI did not degrade, however, no aniline was found in the reaction.

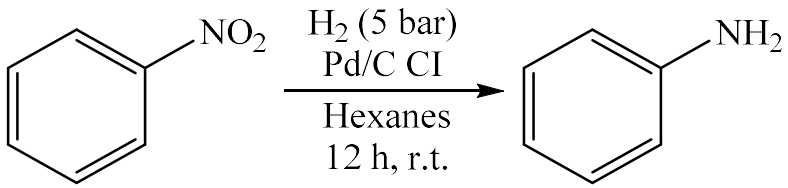

Scheme 3 Reduction of nitrobenzene to aniline in hexanes using hydrogen and a 3D printed CI

The result of catalytic activity being seen in butanol but not in hexanes and the CI degrading in butanol but not in hexanes lead us to believe Pd/C was leaching into the solution. A CI was then left in methanol overnight to degrade the CI. The solvent was the filtered off and was tested for palladium in the solution using ICP-MS. 0.0019 mg of Pd was detected in the solvent indicating that palladium was indeed leaching into the solution when the CI degrades.

We then decided to try a more active functional group towards the hydrogenation with Pd, in hopes of seeing activity in hexanes. We landed on trying to reduce benzaldehyde to benzyl alcohol. We knew that the CI would degrade in butanol so we tried first in hexanes (Scheme 4).

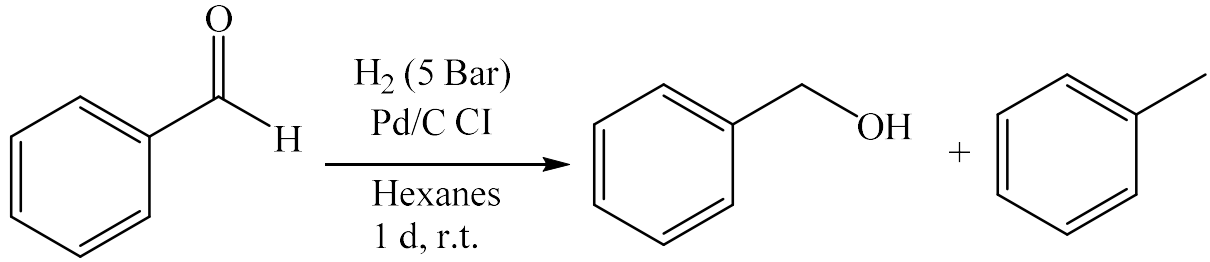

Scheme 4 Reduction of benzaldehyde to benzyl alcohol.

After 1 day the reaction was stopped and analyzed using GC-MS. The results showed a slight production of benzyl alcohol and full reduction to toluene was also seen. The low yield of benzyl alcohol and toluene isn't a representation of the catalysts activity because the catalyst is known to be highly active towards these reductions. The low yield can be explained by the small amount of Pd that is exposed on the surface of the CI. The benzaldehyde was also analyzed by GC-MS to make sure no benzyl alcohol was present and none was seen. The background reaction then was done with a CI with no Pd/C added (Scheme 5). No production of benzyl alcohol was witnessed.

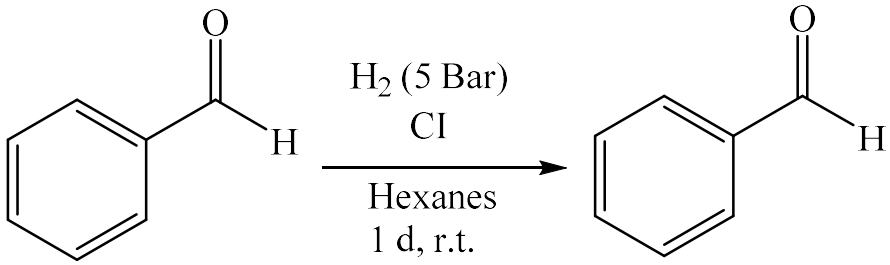

Scheme 5 Background reaction of the reduction of benzaldehyde to benzyl alcohol.

We then wanted to see if the conditions were pushed would more conversion to benzyl alcohol be seen. A steel parr-bomb was then used for this reaction. A CI was placed inside the parr-bomb reactor along with hexanes and benzaldehyde. The vessel was then pressurized to 40

bar with hydrogen and heated to 40 °C for 1 day (Scheme 6). After a day the reaction was analyzed by GC-MS and showed an increase in the produciton of benzyl alcohol and toluene.

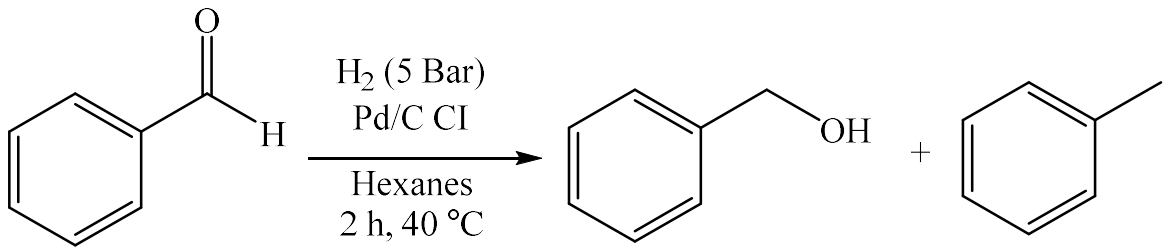

Scheme 6 Reduction of Benzaldehyde with hydrogen in a parr-bomb.

This result lead us to move towards harsher conditions for the 3D printed reaction vessel. We wanted to see then if the reaction vessel was heated with a sand bath would heat be able to transfer to the solvent inside the vessel. We set the vessel in a sand bath and heated the sand bath to 55 °C and recorded a temperature of 45°C inside the vessel. Also, no adverse affects were seen by heating the reaction vessel.

We set up the same reacton of the reduction of benzaldehyde in hexanes in the 3D printed reactor (Scheme 7). The first step was to pressurize the reaction vessel to 5 bar with hydrogen. The vessel was then set inside the sand bath, which was set to 55 °C. However, once the temperature reached the 55 °C the bottom of the vessel ruptured. We went past the limits of the 3D printed reaction vessel and it was then decided to not heat the 3D printed reaciton vessel while pressurizing again.

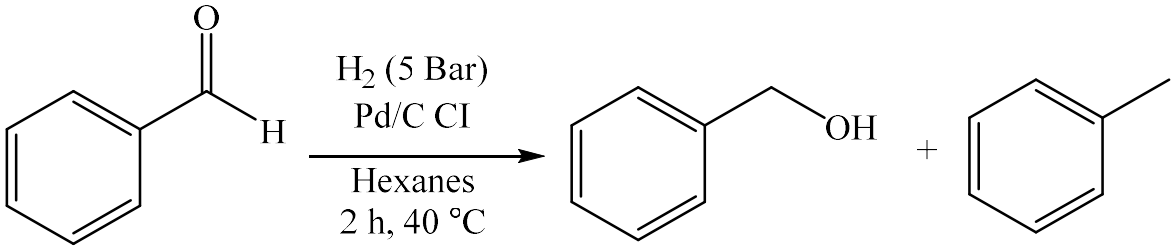

Scheme 7 Reduction of benzaldehyde with H_2 while heating the 3D printed reaction vessel

We then went back and redesigned the reaction vessel now knowing that the weak point is the flat bottom. We decided that to strengthen the vessel it would be optimal for the bottom to be rounded (Figure 13). It should show similar characteristics to glassware where a round bottom flask is ideal for holding pressure compared to a flat bottom flask.

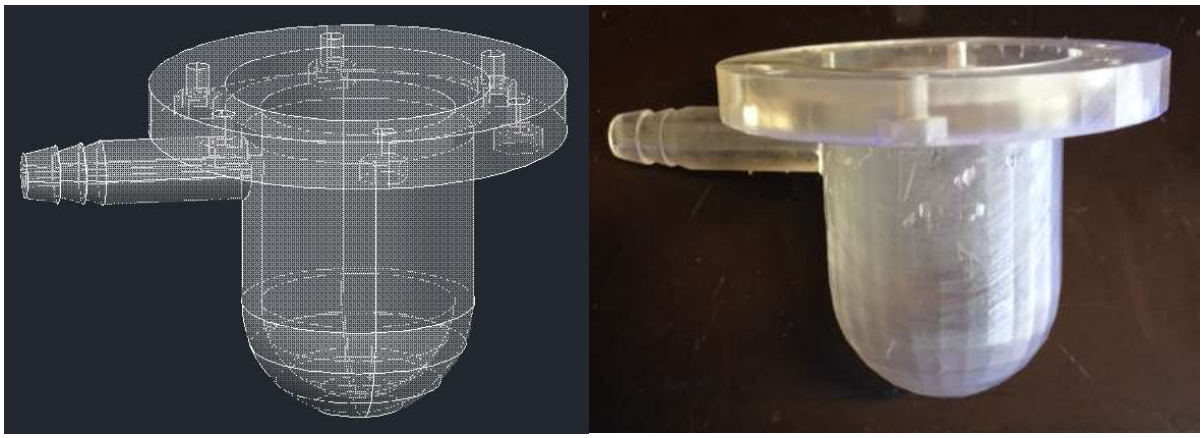

Figure 13 Round bottom reaction vessel (Left) – AutoCAD image (Right) – 3D printed object

Now that we have a stronger vessel it is time to explore other compounds to reduce. The future of this project now lays on trying electron withdrawing and electron donating aldehydes. Hopefully more active substrates will show a higher yield.

Conclusion

In conclusion we have successfully printed the first 3D printed object with a metallic catalyst incorporated into the print. This catalyst went on to give slight conversion of benzaldehyde to benzyl alcohol and toluene at room temperature and 5 bar of hydrogen. This would be the first known example of a 3D printed catalyst being active for the reduction of aldehydes. Along with the 3D printed catalyst, a fully 3D printed reactor has been designed and printed that is able to hold pressure up to 5 bar and retain the seal. The limit of this reactor was found to be 5 bar and heating hexanes to a temperature of 45 °C. This reactor is significant due to the sturdiness of the object and the cost taking to make it. The resin used costs $0.15 per mL and

the entire reaction vessel consists of 62 mL of resin, so the complete reaction vessel costs $9.24 to print. This shows that 3D printing could result in a very cost effective route compared to the alternative custom reaction vessels costing in the hundreds of dollars. 3D printing is an exciting new technology that has almost unlimited applications with the right material being printed. These materials and applications are what will be highly sought after in the chemical world. The 3D printed catalyst is only the start of what is possible with 3D printing and heterogeneous catalysis.

Experimental

Materials. Purchased Formlabs 1+ 3D printer from formlabs. Clear resin was also purchased from formlabs and the resin tanks used were provided with printer. The Pd/C (10 wt%), diphenylacetylene (98%), nitrobenzene , and 4-nitrobenzonitrile (97%) were all purchased from Aldrich with no further purification.

Catalyst insert with Pd/C. Clear resin (100 mL) was added to the resin tank for a Formlabs 1+ 3D printer. Directly to the resin Pd/C 10 wt% (0.300 g, 0.28 mmol Pd) was added. Using a plastic spatula the Pd/C was mixed until appearing evenly distributed throughout the resin. From there the catalyst cap was printed at a 45° angle with supports (0.7 density, point size of 0.2 mm) until layer 650. The print was then paused and the resin tank was switched with one that contained only clear resin at which time the print was resumed. To remove the residual resin from the print it was submerged in an iPrOH bath for 2 min. After the 2 min. the print was taken out and the supports were removed. The print was again submerged in the iPrOH bath for 8 min and then washed with new iPrOH. It was then let dry for 15 min.

Reduction of nitrobenzene To the 3D printed reaction vessel 10 mL of solvent was added followed by nitrobenzene (0.200 mL, 0.002 mol). The porous box CI was screwed into the top of

the reaction vessel, which was then screwed down onto the bottom of the reaction vessel and sealed by the rubber gasket. From there the vessel was purged with a flow of hydrogen. Once purged the vessel was sealed by screwing tight the pressure release insert. Upon sealed the vessel was pressurized with 5 bar of hydrogen and let stir at room temperature for 1 day. The reaction was then analyzed using GC-MS.

Reduction of benzaldehyde To the 3D printed reaction vessel 10 mL of solvent was added followed by benzaldehyde (0.200 mL, 0.002 mol). The porous box CI was screwed into the top of the reaction vessel, which was then screwed down onto the bottom of the reaction vessel and sealed by the rubber gasket. From there the vessel was purged with a flow of hydrogen. Once purged the vessel was sealed by screwing tight the pressure release insert. Upon sealed the vessel was pressurized with 5 bar of hydrogen and let stir at room temperature for 1 day. The reaction was then analyzed using GC-MS.

References

1. Karl S. Wagner. (2014) *Investigate Methods to Increase the Usefulness of Stereolithography 3D Printed Objects by Adding Carbon Nanotubes to Photo-Curable Resins*. University of Minnesota Duluth. *SCSE-Mechanical and Industrial Engineering UROP Papers*
2. Simon J. Leigh,* Robert J. Bradley, Christopher P. Purssell, Duncan R. Billson, and David A. Hutchins *PLOS ONE* **2012**, *7*, 1-6
3. Maxim Lobovsky, Alexander Lobovsky, Mohammad Behi, and Hod Lipson Cornell. *Solid Freeform Fabrication of Stainless Steel Using Fab@Home*. (2008) University Engineering Learning Initiatives (ELI)

4. Yong Lin Kong, Ian A. Tamargo, Hyoungsoo Kim, Blake N. Johnson, Maneesh K. Gupta, Tae-Wook Koh, Huai-An Chin, Daniel A. Steingart, Barry P. Rand, and Michael C. McAlpine*. *Nano Lett*. *2014*, *14*, 7017-7023.
5. Philip J. Kitson, Mali H. Rosnes, Victor Sans, Vincenza Dragone, and Leroy Cronin*. *Lab Chip*, **2012**, *12*, 3267-3271
6. Mark D. Symes, Philip J. Kitson, Jun Yan, Craig J. Richmond, Geoffrey J. T. Cooper, Richard W. Bowman, Turlif Vilbrandt and Leroy Cronin*. *Nature Chemistry*, **2012**, *4*, 349-354.
7. Philip J. Kitson, Mark D. Symes, Vincenza Dragone and Leroy Cronin*. *Chem. Sci*. **2013**, *4*, 3099-3103.
8. Philip J. Kitson, Ross J. Marshall, Deliang Long, Ross S. Forgan*, and Leroy Cronin*. *Angew. Chem. Int. Ed*. **2014**, *53*, 1-7.
9. Vincenza Dragone, Victor Sans, Mali H. Rosnes, Philip J. Kitson and Leroy Cronin*. *Beilstein J. Org. Chem*. **2013**, *9*, 951-959.
10. Kari B. Anderson, Sarah Y. Lockwood, R. Scott Martin, and Dana M. Spence*. *Anal. Chem*. **2013**, *85*, 5622-5626.

CHAPTER 4

GENERAL CONCLUSIONS

In summary, we were able to prepare the first heterogeneous zinc catalyst for the hydrosilylation of carbonyl containing compounds. MSN-ZnOEt was prepared from the deprotonation of the silanol groups on the surface of MSN with $ZnEt_2$ followed by a reaction with EtOH. MSN-ZnEt and MSN-ZnOEt have been characterized using FTIR, ICP-MS, TEM, and chemisorption. The ICP-MS in itself proved that there was zinc immobilized on the surface of MSN. This catalyst was then able to go on and successfully catalyze the hydrosilylation of ketones, aldehydes, esters and enones with good percent conversions and good percent yields. It was found that $(EtO)_3SiH$ was the best reducing agent when reacted with MSN-ZnOEt and acetone. There was also no solvent effect to be found for the hydrosilylation of acetone.

This MSN zinc complex was also found to react with *tert*-butylhydroperoxide to form the peroxide on the surface of MSN (MSN-ZnOO^{t}Bu). This was proved by the stoichiometric reaction between MSN-ZnOO^{t}Bu and PPh_3 resulted in the formation of the oxide. This reactivity of MSN-ZnEt then lead to the catalytic epoxidation of α,β-unsaturated ketones with *tert*-butylhydroperoxide.

Lastly, we have successfully designed a 3D printed reactor using SLA printing that is able to have reagents added, removed and also to hold a hydrogen pressure of 5 bar. The custom reactor can be adapted to any specifications that are needed and fit within the build area of the printed. Furthermore, we have produced the first 3D printed structure containing an organometallic catalyst. This 3D printed catalyst showed activity for the reduction of benzaldehyde to benzyl alcohol and toluene.